Evidence for Mesozoic shear along the western Kunlun and Altyn-Tagh fault, northern Tibet (China)

Nicolas Arnaud, Paul Tapponnier, Roger Françoise, Maurice Brunel, Urs Schärer, Wen Chen, Xu Zhiqin

Evidence for Mesozoic shear along the western Kunlun and Altyn-Tagh fault, northern Tibet (China).

N. Arnaud[1], P. Tapponnier[2], F. Roger[3], M. Brunel[4], U. Scharer[3], Chen Wen[5], and Xu Zhiqin[5].

1: UMR 6524 CNRS Clermont-Fd, France; 2: IPG Paris et Univ. Paris 7, France; 3: URA1093 CNRS Paris, France
4: Univ. Montpellier 2 et URA1763 CNRS, France; 5: Inst. of Geology, CAGS Beijing, China

Abstract

The strike slip faults of North Tibet accommodate part of the Cenozoic convergence between India and Asia. Along the Karakax valley south of Yecheng and near the Xidatan trough south of Golmud, the active traces of the Altyn-Tagh and Kunlun faults follow narrow belts of metamorphic rocks. The deformation recorded in those mylonites is sinistral strike slip. Rb/Sr and $^{40}Ar/^{39}Ar$ ages of deformation from syn-tectonic fabrics formed at 350-400°C 120 Ma ago. Argon loss suggests that deformation was associated to a 250-300°C thermal pulse that lasted 5 to 20 Ma after the onset of movement. Unroofing occurred much later, around 25 Ma ago when sudden cooling suggests a component of thrusting or more likely normal faulting. The Cretaceous shear may be related to collision between the Qiantang and Lhasa blocks. The Karakax and Xidatan shear zones may have formed a unique, continuous boundary in the Cretaceous, which was later reused by the Tertiary strike-slip faults, leading to potentially calculable offsets along the Altyn-Tagh fault.

Large active faults of Northern Tibet may have accommodated a significant part of the deformation due to collision between India and Asia. The kinematics and magnitude of Cenozoic displacements along these faults have been the focus of abundant research [*Tapponnier and Molnar*, 1977, *Peltzer and Tapponnier*, 1988, *Avouac and Tapponnier*, 1993, *Peltzer et al.*, 1988, *Molnar and Kidd*, 1988, *Meyer et al.*, 1996, 1998, *Van der Woerd et al.*, 1998], but these study have essentially not addressed the problem of pre-Cenozoic activity of these faults. Due to a lack of geological and reliable geochronological data, very little is known about the structural history of these faults prior to 30 Ma. Such a knowledge, however, is essential to reconstruct the geodynamic evolution of the Asian continent in Phanerozoic times as well as the Tertiary finite displacements induced by the India-Asia collision using older piercing points.

Here we present geochronological data along two segments of the Altyn-Tagh and Kunlun faults system, near 75° and 100°E respectively. We first briefly summarize the geology of the two regions sampled, then the ages and cooling histories both on a local scale and on a broader scale to document the existence of Mesozoic movement along both faults and the possible Tertiary offset of the metamorphic rocks on the Altyn-Tagh fault.

I/ Present geological setting.

Sampling area are located (figure 1) roughly parallel to the structural limits of the northern topographical limit of the Tibet

Plateau. In the east, we sampled metamorphic rocks along the Kunlun fault south of Golmud over a distance of roughly 100 km. A geological description of the Golmud section is given in *The geological evolution of Tibet, Phil.* by the Royal Society of London (1998). In the west we sampled metamorphic rocks along the Karakax valley, over a distance of c.a. 100 km following the south flank of the Kunlun mountains south of Yecheng. A geological and geochronological description is given in *Matte et al.* [1996] and *Mattern et al.* [1996].

1- The Kunlun fault in eastern Kunlun.

South of Naji Tal within the eastern Kunlun (figure 2), a step-over between overlapping segments of the Kunlun fault created the impressive Xidatan-Dongdatan pull-apart *trough* [*Van der Woerd et al.*, 1998]. North of this trough, Permian to Jurassic flysch and coal shales are intruded by calkalkaline granites and associated rhyolites. The granitic bodies just north of the fault appear to be largely of Triassic age [*Harris et al.*, 1988, *Mock et al.*, 1998]. South of the fault, the geology is dominated by the steep isoclinally folded slates and phyllites of the triassic series of Bayan Har terranes, the western equivalent to the famous Songpan Garze flysch sequence on Qiantang block. In the Xidatan valley, the fault bounds the southern flank of the Kunlun range and limits the Kusar Hu Neogene basin. It is marked by steep triangular facets indicating a normal component of throw. A belt of pegmatites, mylonites of granite and leucogranite, garnet schist phyllonites of various sedimentary origins, up to one kilometer wide, is intermittently exposed along the northern footwall of the Kunlun flank. The rocks show steep N100-110 striking schistosity planes roughly parallel to the fault, with horizontal lineations and clear sinistral shear indicators (figure 3). A petrographic study of the ductile deformation of quartz and the recrystallization of muscovites suggest peak deformation temperatures of ca 350-400°C *[Brunel and Geyssant, 1978]*. Such ductile fabrics are particularly well exposed to the west where the facets on the mountain sides are well developed and normal throw prominent.

2- Western Kunlun range: the Karakax valley.

The Karakax river follows the westernmost segment of the Altyn-Tagh fault about 80 km between Sanshili and Kanshiwar (figure 4). The river is offset about this amount by the fault which continues westward to the Muztagh Ata Tagh and Kongur Shan [*Brunel et al*., 1994]. The Karakax river then escapes towards the Tarim basin in a narrow gorge approximately at 78°E. The active trace of the fault is particularly clear in this area with glacial and post-glacial terrace rivers offsets, seismic mole tracks and kilometer-long pull-aparts and push-ups [*Peltzer et al.*, 1996, *Matte et al.*, 1996]. North of the fault, the southern flank of the western Kunlun range exposes a volcanic arc sequence sheared with other rocks along the fault. Tectonic slices of pyroxene cumulates, gabbros and basalts, granodiorites and granites, granulites and amphibolites, and Talc and jadeitic pyroxene are thus juxtaposed over a width of 2 to 3 km [*Matte et al.,* 1996]. The highest summits of the range expose leucogranitic bodies. Regional U/Pb, Rb/Sr and Ar/Ar geochronological data indicate mid-Paleozoic, 380 Ma, and post-Triassic (200 Ma) suturing events [*Matte et al.*, 1996, *Arnaud*, 1992, *Xu et al.*, 1996]. The fault bounds a region of folded slates, to the south, with a facies similar to the Bayan Har slates. To the southwest of Kanshiwar, Triassic granites become progressively sheared toward the fault. Such mylonitic granites, together with garnet-muscovite schists and leucogranitic lenses in the highly sheared zone along the corridor bear evidence of syntectonic recrystallization (micas). Steep N100°-120° foliation planes bear horizontal lineations . The shear sense is sinistral in the micaschists but variable or less clear in other rocks [*Mattern et al.* 1996, *Matte et al.* 1996] and temperatures of deformation are of the order of 350-400°C.

II/ Geochronology.

1- Analytical techniques.

For U/Pb and Rb/Sr dating, mineral separates were obtained by processing 1-2 kg samples through crushing, the disk-mill, the Frantz magnetic separator and heavy liquids.

For each analysis, the fractions were selected grain-by-grain to represent the entire range of crystal types present in the population. Zirconswere mechanically abraded (Krogh, 1982) prior to dissolution in polytetrafluoroethylene (PTF) Teflon bombs with > 50% HF at 220°C for 2-3 days (Krogh, 1973), and feldspar, whole rock and micas were dissolved in two steps, using > 50% HF followed by 6N HCl, both at 150°C. U-Pb and Rb-Sr analyses were performed by the isotope dilution method using a ^{205}Pb-^{235}U-^{233}U and a ^{85}Rb-^{84}Sr mixed isotope tracer, respectively, and isotope ratios were measured on a Cameca TSN 206 mass spectrometer, equipped with a single Faraday collector and a secondary electron multiplier for U, Pb and Rb, and a double Faraday collector for Sr. The decay constants used for U and Rb are those recommended by IUGS (Steiger and Jäger, 1977). For Sr standard NBS 987 an average value of ^{87}Sr/^{86}Sr = 0.71024 ± 3 (2σ, n = 25) was obtained. Analyses of the NBS 983 standard yield a mean mass fractionation value of 0.1 ± 0.05% amu-1 for both the Faraday and secondary electron multiplier systems. Sr ratios were normalized to ^{86}Sr/^{88}Sr = 0.1194.Total blanks lie around 10-15 pg for Pb and at < 1pg for U, whereas blanks for Rb and Sr are negligible. All zircon analyses were also corrected for initial common Pb, the isotopic compositions were determined from Stacey and Kramers (1975) at 384 Ma. Calculations were made using the Isoplot 200 program of Ludwig (1987). Analytical uncertainties are listed as 2σ and uncertainties in ages as 95% confidence levels.

For ^{40}Ar/^{39}Ar dating purposes, high purity aliquots were separated using heavy liquid, magnetic separator, and hand-picking methods. Minerals in the range 180-250µm were always used. Because samples were sampled and analysed at different times between 1990 and 1996 they were irradiated at different periods, but always in the site 69 of the Siloée reactor in the Grenoble facility of the Commissariat à l'Energie Atomique (France). They were shielded by cadmium foil to reduce neutron interactions on ^{40}K, with CaF_2 and K_2SO_4 to account for interfering nuclear reactions, and flux monitors in the upper and lower positions in each vessel. Most of the time the Caplongue hornblende (344.5 Ma, *Maluski and Schaeffer*, 1982) was used as a flux monitor. Step heating analysis was performed at the ^{40}Ar/^{39}Ar laboratory in Clermont-Ferrand on a VG3600 mass spectrometer. The major characteristic of our facility is that analyses are carried out successively on two collectors: a Faraday cup of 10^{11} ohm in axial position and a photomultiplier that receives the signal of a Daly plate interceptor. Using both collectors allows for greater amounts of gas to be analysed when ^{36}Ar signals are low, while bigger signals for ^{39}Ar and ^{40}Ar are taken on the Faraday cup. This decreases the errors on the low signals. Duplicate analyses of ^{39}Ar during each run allows to calculate the gain between Faraday and photomultiplier signals. For signals of more than 20mV (with a sensitivity of 3.15×10^{-17} mole/mV) on the Faraday cup, statistical analysis of more than 2000 gain analyses shows good reproducibility at 92.5 with an estimated error of 2% maximum. This error is taken into account during age calculation. Average blanks for ^{40}Ar range from 1.3×10^{-15} moles STP at low temperature to 4.7×10^{-15} moles STP at 1200°C on both furnaces and have been reproducible along the years. Blanks for other masses are usually under detection level or so low that they have large uncertainties. Age spectrum calculations are given at 1σ on each step and include all correction factors, as well as 2% errors on blanks taken for correction. Individual steps do not include error on J factor, while plateau and isochron ages do so, with an average of 1.5%. Comparison of several isotopes allows qualitative analysis of K/Ca (^{39}Ar/^{37}Ar) and Cl/K (^{38}Ar/^{39}Ar) ratios. Note that for simplicity K/Ca and Cl/K will be used in the text while no strict calculations have been made and those terms only reflect the isotope ratios. Results are given in table 1. Plateau ages and isochrons are calculated following the criteria of *Dalrymple et al.* [1981] and *Roddick* [1980].

2- Age of deformation events.

Because argon systematics show evident losses in the temperature range 300 to 450°C it is often difficult to distinguish the

dating of deformation from that of cooling subsequent to the peak of deformation. In our case the characteristics of plastic deformation of quartz show features of dynamic recrystallization such as sub-basal deformation lamellae [*White, 1976*], typical of low temperatures of deformation in the range 300-350°C [*Brunel and Geyssant, 1978*]. U/Pb dating will thus yield the emplacement age as an upper limit for the thermal history of these rocks. Rb/Sr and Ar/Ar ages will be only partially retained by magmatic muscovite, but will be very close to the deformation age on syntectonic muscovites since their closure temperatures are on the order of the highest bracket [*Lister and Baldwin*, 1996, *Hames and Bowring*, 1994]. Finally the Rb/Sr and $^{40}Ar/^{39}Ar$ ages of biotites however will date subsequent cooling since their closure temperature is lower [*Harrison et al.,* 1985].

a. The Kunlun fault in eastern Kunlun. Only limited data is available for magmatic ages of the widespread plutonic activity. *Harris et al.* [1998] show dominantly Mesozoic ages and more rarely Paleozoic ones. We dated one deformed granite (QGS17, figure 5 and table 1) from the belt of metamorphic rocks on the northern side of the fault (figure 2). The deformation of this rock has resulted in an orthogneiss in which magmatic biotites and muscovites are not recristallized. The U-Pb data for the Xidatan orthogneiss (QGS 17) are shown on a Concordia diagram *[Wetherill, 1956]* in figure 5. The zircons selected for U-Pb analysis were euhedral, unbroken, crack-free crystals, translucent and inclusion free. Eight fractions were made using color, shape (euhedral or rounded) and size criteria ; their weight ranges from 0.059 mg to 0.1 mg. The data define a reverse discordia, with a lower intercept at 384 ± 9 Ma and an upper intercept at 2.4 ± 0.2 Ga, when plotted on a concordia. The most discordant fraction corresponds to rounded fractions and demonstrates inheritance from an old basement.

Rb/Sr dating of the same rock (figure 6a and table 2) on whole rock, K-feldspar, and three different size fractions of biotite and muscovite are analyzed for Rb-Sr, define two scattered isochrons. Data for whole rock, K-feldspar, and muscovite fractions define an isochron of 197 ± 3 Ma (± 2σ) with an initial $^{87}Sr/^{86}Sr$ ratio of 0.7312 ± 0.0006 while the whole rock, K-feldspar and biotite fractions array yield a date 114 ± 2 Ma (± 2σ) and an initial Sr ratio of 0.7359± 0.0002. This indicates one or two successive isotopic remobilisation and therefore thermal events.

Another rock, a deformed pegmatite, was also dated by Rb/Sr (QGS 16, figure 6b). Feldspar and 4 muscovites yield an array with an date of 192 ± 12 Ma and an initial ratio $^{87}Sr/^{86}Sr$ of 0.7138 ± 0.0001 (± 2σ).

Note that in both samples the initial Sr ratios are similar. The highly radiogenic initial 87Sr/86Sr ratios for biotite and muscovite isochrons, show that the major source lithology of the granite was derived from highly evolved continental crust.

$^{40}Ar/^{39}Ar$ dating has been carried out on several facies (figure 7 and table 3) from the metamorphic band north of the fault. Because most of the deformed granites are calk-alkaline in chemistry and thus have no primary muscovites, the latter are associated only with syn-tectonic recrystallization. Though biotites probably predate the deformation, most appear to have recrystallized in shear bands along the shear S/C planes, and are plastically deformed suggesting they recorded post-emplacement tectonic events. Sample K93G30 comes from the highly sheared edge of a granite intrusion in the middle of Xidatan trough. Sinistral mica-fish shaped muscovites yield a climbing age spectrum, from ages of ca. 51 Ma up to a plateau at 120 ± 2 Ma covering 75% of the total ^{39}Ar. The last steps are a little older at 128 Ma probably as a result of undercorrection of ^{40}Ar high temperature blanks. No sign of excess argon or unusual behavior was noted in this sample, though amounts of radiogenic argon (more than 90% in most degassing steps) precludes the use of isotope correlation plots [*Roddick*, 1980].

The other samples, K93G36, K93G37 and K93G42 were sampled further west in a steep and narrow orthogneiss band just north of the active fault trace. The gneisses bear clear sinistral indicators on vertical foliation

planes with horizontal lineation and sinistral shearing indicators. Sample K93G36 contains both biotites and muscovites, both underlining the metamorphic foliation. We obtain simple spectra with a large plateau at 126.8±3.5 Ma for the muscovite and a much younger one for the biotite at 93.4±1.1 Ma. A difference in age between micas is not unusual as the biotite closure temperature is probably at least 50°C below that of muscovite, but this one is particularly large, suggesting very slow cooling. This is consistent with the first step of the muscovite spectra being younger than the plateau. Sample K93G37 is a leucocratic mylonite and in which both the muscovite and biotite yield very well developed plateaus at 122 ± 1 Ma and 111 ± 2 Ma, with the first step younger than the plateau for the muscovite. Again biotite is younger than muscovite. Finally, sample K93G42 is a sheared pegmatite with a plateau age on muscovite of 120.1 ± 3.5 Ma, with again a younger first step.

All together, these results suggest that middle Paleozoic plutons were at roughly 350-400°C during Cretaceous time. Keeping in mind the relative closure temperature for muscovites and biotites for Rb/Sr (500°C and 300 °C) [*Cliff*, 1985] and $^{40}Ar/^{39}Ar$ (400°C, 325°C) [*Lister and Baldwin*, 1996; *Hames and Bowring* ,1994] and the temperature of deformation as deduced from petrography (350-400°C) it appears that this set of ages can be interpreted in two ways. On the one hand the various ages represent a cooling curve sampled at several moments in an otherwise rather monotonic cooling history after a tectonometamorphic event at least as old as the oldest ages, thus triassic. On the other hand, those distributed ages can represent disturbance of the geochronometers, first closed during at least Triassic times, by a post-triassic deformation event along the fault, possibly as young as the youngest ages, thus cretaceous Although ages in the range 190-200 Ma are reported elsewhere [*Delville et al.*, 2001; *Mock et al.*, 1999; *Roger et al.*, submitted] for deformation as well as magmatic activity it is not possible to at present to choose between those equally plausible solutions.

b. The western Altyn-Tagh fault. Direct dating of the shear deformation along the fault was possible on garnet-muscovite micaschists (K89G217) bearing horizontal lineation and sinistral indicators clearly associated to fault movements. Syn-tectonic muscovites in the shearing planes were dated (8a and 8b). A well-defined plateau appears on more than 90% of total ^{39}Ar released with an age of 119±2 Ma. The first steps have significantly lower ages from 83 to 95 Ma associated to lower though not unusually so K/Ca ratios though. The last step shows a higher age that is probably due to under correcting of blanks at 1400°C accounting for almost 40% of the total ^{40}Ar released at that step.

In order to place constraints on the thermal conditions of the deformation, rocks near the shear zone along the fault that did not completely recrystallize corridor were sampled. Closing toward the fault, biotites from a foliated granodiorite (sample K89G204) taken a few hundreds of meters north of the fault yields a disturbed spectrum with, at the beginning, ages increasing from 166 Ma to ca. 400 Ma, then a median bulge at 450 Ma, and finally a small pseudo-plateau at 420± 4 Ma with 50% of the total ^{39}Ar. The bulge is older than most Paleozoic intrusives in the western Kunlun range (350 to 400 Ma on average [*Matte et al.*, 1996, *Arnaud*, 1992]. Moreover, this bulge correlates with a negative spike in the K/Ca ratio and a positive one for the Cl/K ratio. This situation matches that described by *Ruffet et al.* [1991], who conclude to the presence of chlorite interlayered with the biotite, in agreement with our petrographic observations. It is thus likely that the minimum ages at the beginning of the spectrum are partially due to excess ^{39}Ar in low retentivity sites of the biotite lattice. However, the magnitude of the drop in ages at the beginning being more pronounced than the excess ages in the middle, a real age gradient probably exists in this sample, with an argon loss at a time younger than 200 Ma ago.

Farther east, muscovites from leucogranitic boudins within schists just south of the active fault trace, and with the same fabric (K89G44), have an even more complex spectrum (figure 8a). The first two steps are

clearly affected by excess argon (increasing Cl/K ratio), then ages climb from 94 Ma to a broadly defined plateau at 150±3 Ma (for 58% of released ^{39}Ar) before finally climbing to 177 Ma. The last much higher step must be regarded with caution because it is probably affected by blank correction. Variations in age seem to correlate with K/Ca variations which suggest mineralogical heterogeneity. The inverse isochron plot is scattered but not correlated enough to distinguish between a possible excess component and a real age gradient. Overall, this spectrum suggests that the argon system was partially reset around 100 Ma from a much older sample. The ill-defined plateau age and the highest age, however are both coherent with the Mesozoic history in this area.

Finally sample K89G42 (figure 8b) is a undeformed granite taken a few kilometers south from the fault in the middle of the Songpan Garze flysch. Muscovites and biotites show almost undisturbed spectra at 190 ± 8 Ma and 177 ± 3 Ma respectively suggestive of slow undisturbed cooling.

These results are most simply interpreted in a way similar to the eastern Kunlun in Xidatan. It appears that a major thermotectonic event occurred during Triassic times, and that rocks along the fault have recorded either monotonic and slow cooling between the Trias and the Cretaceous, or alternatively that deformation at Cretaceous times along the Altyn-Tagh fault in the Karakax induced resetting of geochronometers along the fault. It is noteworthy that apparent progressive resetting of ages when nearing the fault favors the latter interpretation.

3- Thermal history and cooling along the faults.

To unravel in more detail the thermal history associated to the ductile fabrics, whatever its age, and subsequent cooling, simple diffusion models were tested on partially reset micas to bracket the magnitude and duration of the thermal event associated with Cretaceous fault movement. Analysis and modelling of K-feldspar data was conducted following the method developed by *Lovera et al.* [1989, 1991]. To compute theoretical argon losses we used published data from diffusion studies on micas. For the biotite, we took the values chosen by *Harrison et al.* [1985] with a cylindrical geometry (activation energy E= 47 kCal/mol, frequency factor D_o=0.077cm^2/s, and characteristic diffusion radius r =150µm which leads to an average closure temperature of 325°C). For the muscovite, recent contributions by *Lister and Baldwin* [1996] and *Hames and Bowring* [1994] disagree on diffusion geometry and kinetic values resulting in a 50°C difference in the closure temperatures. For the coherence of the data with biotites we took values of the latter authors (E= 52 kCal/mol, D_o=0.04 cm^2/s and r=150 µm which transfer into a closure temperature of 398°C).

a. The Kunlun fault. Petrology and dating imply conditions of 350-400°C to have prevailed at ca. 120 Ma. Some muscovites spectra show apparent argon loss shapes, with the first steps significantly younger than the plateau. In many cases those decreasing age steps seem associated with decreasing K/Ca ratios but optical examination did not reveal severe alteration at rims or in defects, nor any reaction rims. Moreover the K/Ca ratios are always greater than 10 and up to 100 even in the beginning of the spectra. Consequently those spectra were used as indicative of temperature/time conditions. It is noteworthy that the biotites that appear to be kinematically coeval with the muscovites are systematically younger implying thatcooling in biotites was systematically delayed c.a. 20 Ma before compared to muscovites. This delay is particularly long and suggests abnormal cooling conditions or even thermal stasis after muscovite closure. Those conditions were calculated by comparing the integrated total ^{40}Ar/^{39}Ar ratio on muscovites (corresponding to the total fusion age) and the plateau age defined on high temperature steps and assumed to be close to the original age. For example sample K93G36 shows 1.8% loss and sample K93G30 2.6% loss. Moreover biotites ^{40}Ar/^{39}Ar ages are always significantly younger than the muscovites though significant variations among their ages are observed. It is easy to calculate possible losses induced by varying (temperature time)

pairs (figure 9) and this leads to estimations of temperatures roughly 250-300°C lasting for 5 to 20 Ma. Therefore, one concludes that a significant thermal regime was maintained in the fault zone for the period 120-100 Ma.

The data from K-feldspars appear compatible with those conclusions. On both samples K93G36 (figure 10a) and K93G30 (figure 10b), the feldspars age spectra show increasing ages to maxima of 86 to 89 Ma. With use of the multidomain theory, several authors have suggested that the most retentive diffusion domains in feldspar have a closure temperature close or even higher than that of biotites. Similar ages of the biotites and feldspars in our case further support this idea. Moreover, even if a broader estimate of closure temperature for feldspars is taken roughly around 250°C, the maximum age of the feldspars leads to the idea of a long lasting thermal event when compared to that of the muscovites. If both spectra show increasing ages they differ from one another, as K93G30 is monotonously increasing while K93G36 shows a small plateau in the first 40% of ^{39}Ar release at 26 Ma. In each case the first steps are associated to very low ages of less than 10 Ma. Several studies [*Arnaud and Kelley*, 1997; *Parsons et al.*, 1988] have suggested possible artifacts in the early stages of degassing of feldspars, in which complex sub-solidus textures are likely to express in the first percents of gas released. Thus the first 5% of the ages spectra are not taken into account in our modeling. The inverse isotope diagram fails to show any systematic behavior and suggests that the age range is real. Overall, K/Ca and Cl/K plots show a remarkable homogeneity, particularly the near absence of plagioclase mixing or fluid inclusion degassing. Therefore, such spectra are most likely the result of partial ^{40}Ar loss by a secondary heating event or continuous loss associated with slow cooling. No metamorphic or magmatic phase is reported in this region of the Eastern Kunlun during the Cenozoic and *Mock et al.* [1999] indicate that feldspar spectra similar to those presented here are common in the Eastern Kunlun and are not spatially linked with any pluton or visible structural feature. It is likely therefore that such argon loss spectra are indicative of slow cooling superimposed on a multidomain structure as experimental degassing reveals on associated arrhenius plots. The model of K93G36 suggests an increasing but overall slow cooling rate of ca 2°C/Ma during the Cenozoic with a rapid change to cooling rate of more than 40°C at roughly 25 Ma. This cooling history is the same as the one obtained from the modelling of the spectra of the K-feldspars from sample K93G30 and is fully compatible with with the mica argon data as well as with fission track regional ages on apatites at 20 Ma [*Lewis*, 1989] though one must note that the latter were not acquired on the same samples.

b. The western Altyn-Tagh fault. The muscovite from K89G44 from (leucogranitic boudins) shows a distinct loss spectra which implies about 5% of radiogenic ^{40}Ar loss, if one compares the total fusion age (158 Ma) with a possible estimate of initial age for the protolith at 160 Ma. Calculating temperature/time pairs for such a loss with muscovite diffusion data leads to a minimum temperature of 260°C and a probable range of 280-300°C for a heat duration of 0.5-10 Ma. Doing the same with the biotite from K89G204 leads to a similar average loss of 5%. But because the biotite is less retentive for argon than the muscovite, temperatures of 230-240°C are deduced for the same time range. This is in good agreement with the fact that the K89G204 granodiorite is deformed but shows no sign of recrystallization. It is also structurally farther from the most ductile zone than is K89G44.

With that temperature range in mind we now turn toward the garnet-micaschist sample K89G217 (figure 11) which was completely recrystallized during ductile shear along the fault. This sample also shows decreasing ages at the beginning of the spectra which can easily be modeled if one assumes that the sample stayed hot for a long time as was hypothesized for the deformed units near Xidatan. In fact it is easy to model the resulting age spectra if a temperature of 300°C is maintained for at least 5 Ma after a closure onset at 120 Ma. Alternatively slow cooling from 300°C at 120 Ma to 200°C at 80 Ma would also be adequate. K-feldspars were studied on samples K89G204 and K89G50 (figure 12), the latter a less deformed

granodiorite taken east of K89G204. K89G50 spectrum is very complex. After 5% of gas release, clearly dominated by excess argon, the next 20% of ^{39}Ar release gives a small plateau at ca. 38 Ma, then a rapid increase to ages of 350 Ma and finally a decrease to a poorly defined plateau at 250 Ma. The presence of the hump in the middle strongly suggests the presence of excess argon *[Forster et al., 1990]*. However the age of the final steps are coherent with the 350 Ma age of most plutonic bodies in southern Kunlun. Moreover, the first plateau is associated to systematic low values of the K/Ca ratio, and therefore is likely to reveal the degassing of perthitic features from that feldspar. Applying multidomain theory to such a sample might therefore lead to large errors in the deduced cooling history. Thus, though diffusion data in laboratory was satisfactorily modeled, only a trivial cooling history is suggested. But it is worth noting that then end of the modeled cooling shows a suggested temperature of ca. 220°C at 50 Ma, which implies further cooling during the Cenozoic. The same kind of remark applies to sample K89G204 (K-feldspar). The effect of excess argon is even clearer at the beginning of the spectra and probably at the end, even if the highest ages agree with the biotite ages given that closure temperature is likely to be lower. Modeling is close to the original spectra and would also suggest a trivial history with very slow cooling since the granodiorite emplacement. However because the biotite showed traces of partial resetting we believe the spectrum is in fact revealing of a complex partial loss event and maybe slow cooling to explain the lowest ages.

Of course these models are non unique as an infinity of temperature/time pairs can be invoked, but all spectra seem consistent with a rather high temperature of ca 300°C that lasted at least several millions of years if not more in late Cretaceous.

III/ Discussion.

The comparison between the between the Karakax segment of the Altyn-Tagh fault and the Xidatan-Dongdatan segment of the Kunlun fault indicates late cretaceous thermal conditions identical in both regions, although spaced by almost 1500 kilometers. Moreover the rocks studied show a strong deformation event. The two simplest explanations are: (1) that deformation occurred at the oldest recorded times, in the Trias or even earlier and that every other data only record surprisingly coeval cooling over a very wide area, or (2) that deformation happened in late Cretaceous superimposed on plutonic rocks emplaced during Triassic or Paleozoic times..

If slow cooling alone brought the rocks along older faults at the same temperature at ca 120 Ma this implies that exhumation along most of what is now northern Tibet has been fairly homogeneous through the Mesozoic, and particularly that ongoing continental accretion further south, such as the Jurassic accretion of the Lhassa and Qiantang terranes did not disturb this equilibrium. In fact, ongoing work on magmatism and cooling during the Mesozoic in northern Tibet (Roger et al., submitted) shows that cooling is broadly homogeneous along northern Tibet after the Trias. However such an homogeneous cooling is rarely maintained except in cratonic areas. Moreover, along the Karakax valley, it appears that samples are progressively and regularly reset when one closes the fault, suggesting a resetting effect associated with the fault corridor (see for example differences between $^{40}Ar/^{39}Ar$ ages from micas on K89G44 and K89G217). We thus favor the idea that indeed cretaceous deformation was superimposed on older plutonic and metamorphic rocks.

1- Origin of a Cretaceous sinistral shear event along the Kunlun and western Altyn-Tagh faults.

The origin of the possible Cretaceous sinistral shear in northern Tibet is unclear. Major orogenic events of late Mesozoic age in Tibet include the accretion of the the Qiantang and Lhasa blocks, a collision that was over prior to that of India with Asia. *Xu et al.* [1984] interpret a U/Pb age of 171 ± 6 My on gneisses from the northern Lhasa block as dating the accretion of Qiantang and Lhasa blocks. South of Longmutso, in western Tibet, small leucogranitic bodies have been dated at

100 Ma [*Arnaud,* 1992, *Matte et al.*, 1996]. *Xu et al.* [1984] also report ages of 121 Ma for leucogranitic bodies south of Anduo. Various studies [*England and Searle, 1986*; *Murphy et al.*, 1995; *Yin et al.*, 1995, *Matte et al.*, 1996] confirm that some shortening occured in southern Tibet before the India-Asia collision, and there is evidence for overthrusting at 150 Ma in the north-eastern Pamir [*Arnaud et al.* 1993]. Also, the Mongol-Okhotsk ocean closes in northern Mongolia closes around the beginning of the Cretaceous [*Khramov,* 1958, *Enkin et al.*, 1992]. New paleomagnetic evidence [*Gilder and Courtillot*, 1997, *Nadir et al.*, 1998] suggests that by 120 Ma, this ocean was closed. Finally there is growing evidence for late Mesozoic suturing and deformation in the Qinling range. It is possible that such events triggered block reorganisation and strike-slip movements along more ancient welding zones within the part of Asia that had already been accreted, much as the collision between India and Asia now does. However, most of the Mesozoic geological history in Tibet is thought of as resulting from « weak » collisions without much continental deformation.

Alternatively, oblique subduction along the Cretaceous active margin of Asia, several hundred kilometers south of either the Kunlun or western Altyn-Tagh faults, might have dragged the southern part of Tibet much as oblique motion of the Pacific plate relative to North-America now drags slices of the western North-American collage.

It has already been mentioned that age data show a systematic delay between muscovite and biotite closure following the peak deformation. Although this may be due to slow unroofing, the ages of the biotites are highly scattered implying heterogeneous exhumation on a very local scale. Alternatively a high and heterogeneous thermal flux lasting for 20 Ma as modeled could be a better explanation.

The existence of thermal anomalies along major strike slip faults is debated. Although there is only a broad, modest rise in the isotherm across the San Andreas fault [*Lachenbruch and Sass*, 1980, *Scholz,* 1980], there is evidence for fairly large heat anomalies along the Red River Fault [*Leloup et al.*, 1993, 1998, *Schärer et al.*, 1994], the Alpine fault [*Grapes,* 1995, *Scholz et al.*, 1979] and the Altyn-Tagh fault [*Van der Woerd et al.*, 1998]. Shear heating can produce a significant amount of heat [*Fleitout and Froidevaux,* 1980, *Thatcher and England,* 1998, *Leloup et al.,* 1998] and in addition large scale strike-slip fault may provide easy path for convection of fluids in the shallow crust thus leading to heat advection. Finally, along the Red River fault the presence of alkaline magmas indicates partial melting in the mantle beneath the fault. Whatever the intimate, if any, connection between strike slip faulting and mantle melting, those magmas provide a supplementary plausible source for upward advection of heat.

2- Cenozoic cooling along the Xidatan-Dongdatan segment of the Kunlun fault.

Cooling, as revealed by the feldspar cooling curves, seems to have been rather slow until the Miocene. In the eastern Kunlun, a severe increase in the cooling rate occurs at 25 Ma, lasting until 10 Ma. Such a cooling rate of 40°C/Ma is not easily reconciled with simple conductive cooling and requires exhumation, either because of enhanced erosion or due to a vertical component of faulting along the faults. Although telling thrusting from normal faulting by the cooling path alone is not possible, normal faulting clearly occurs now along the fault [*Van der Woerd et al.*, 1998] and may have brought the ductily deformed rocks to outcrop. Since similar studies [*Mock et al,* 1999] in the eastern Kunlun generalize a similar cooling event to the whole region north of the Kunlun fault, we infer that limited normal faulting along the Kunlun fault accommodated regional uplift of the range beginning 25 Ma ago.

IV/ Conclusion.

Firstly our observations confirm that at least some segments of the large Tertiary faults of Tibet follow more ancient features. Similar work in north-eastern Tibet and the Qilian shan suggest that NE trending faults might also locally reuse older structures [*Delville et al.*, 2001]. That both E-W the

Xidatan and Karakax segments of the Kunlun and Altyn-Tagh faults are reactivated implies that they were favorably oriented within the stress field generated by the India-Asia collision [*Peltzer et al.,* 1988]. The amount of Cretaceous shear along both shear zones is unknown, but since such movements happens to have taken place in the same sense as the posterior Tertiary slip, part of the finite offset on the faults is clearly unrelated to the India-Asia collision. Offsets based on pre-Cretaceous percing points will therefore be larger than those due to Cenozoic motion resulting from the India-Asia collision.

Second, the great resemblance in rock types, ages, structure and geodynamic environment along both the Karakax and Xidatan shear zones suggest that they may have formed a continuous belt from western to eastern Kunlun. If it was the case, and if the Xidatan zone can be documented westwards to the Ayakum -Kol region, then restoration of the present day offset between the Karakax and Xidatan zones might indicate on order of several hundreds of kilometers of post-Cretaceous slip along the N70°E trending stretch of the Altyn-Tagh fault zone between the Eastern and Western Kunlun, a value in agreement with independent recent estimates [Ritts and Biffi, 2000]. Much of the offset of this transcrustal marker could have resulted from the India-Asia collision.

Bibliography

Arnaud N.O. and S.P. Kelley, Diffusion mechanisms of Argon in pure gem-quality Orthoclase from Madagascar: Experiments and consequences for Thermochronology. *Geochim. Cosmochim. Acta, 61, 15*, 3227-3255, 1997.

Arnaud, N.O., M. Brunel, J.M. Cantagrel, and P. Tapponnier, High cooling and denudation rates at Kongur-Shan, Eastern Pamir (Xinkiang, China) revealed by ^{40}Ar-^{39}Ar alkali feldspar thermochronology, *Tectonics, 12*, 1335-1346, 1993.

Arnaud, N.O., Apports de la thermochronologie ^{40}Ar/^{39}Ar sur feldspath potassique à la connaissance de la tectonique cénozoïque d'Asie. Etude des mécanismes d'accommodation de la collision continentale, Thèse Doct. d'Univ. Blaise Pascal, Clermont-Fd II : 263 p., 1992

Avouac, J.Ph., and P. Tapponnier, Kinematic model of active deformation in central Asia, *Geophys. Res. Lett., 20*, 10, 895-898, 1993.

Brunel, M., N.O. Arnaud, P. Tapponnier, Y. Pan, and Y. Wang, Kongur Shan Normal fault : type example of mountain building assisted by extension (Karakoram fault, eastern Pamir). *Geology, 22*, 707-710, 1994.

Brunel M. and J. Geyssant J., Mise en évidence d'une déformation rotationnelle Est-Ouest par l'orientation optique du quartz dans la fenêtre des Tauern (Alpes Orientales); Implications géodynamiques. *Revue de Géographie physique et de Géologie dynamique, fasc.4*, 335-346, 1978.

Cliff R.A., Isotopic dating in metamorphic belts, *J. Geol. Soc. London, 142*, 92-110, 1985.

Dalrymple, G.B., E.C. Alexander Jr, M. Lanphere and G.P. kraker, Irradiation of samples for ^{40}Ar/^{39}Ar dating using the Geological Survey TRIGA reactor, *U.S. Geol. Surv., Prof. Paper 1176*, 1981.

Delville N., Arnaud N., Montel J. M., Roger F., Brunel M., Tapponnier P. and Sobel E., Paleozoic to Cenozoic deformation along the Altyn-Tagh Fault in the Altun Shan massif area, Eastern Qilian Shan, NE Tibet China. *GSA special publication* "Paleozoic and Mesozoic tectonic evolution of central Asia - from continental assembly to intracontinental deformation.",194, 269-292, 2001.

England, P., and M. Searle, The Cretaceous-Tertiary deformation of the Lhasa Block and its implications for crustal thickening in Tibet, *Tectonics, 5 (1)*, 1-14, 1986.

Enkin, R.J., Z.Y. Yang, Y. Chen and V. Courtillot, Paleomagnetic constrains on the geodynamic history of China from Permian to Present, *J. Geophys. Res.*, 97, 13953-13989, 1992.

Fleitout, L., and C. Froidevaux, Thermal and mechanical evolution of shear zones, *J. Struct. Geol.*, 2, 159-164, 1980.

Foster, D.A., T.M. Harrison, P. Copeland, and M.T. Heizler, Effects of excess argon within large diffusion domains on K-feldspar age spectra, *Geochem Cosmochim Acta, 54*, 1699-1708, 1990.

Gilder, S. and V. Courtillot, Timing of the North-South China Collision From New Middle to Late Mesozoic Paleomagnetic Data from the North China Block, *J. Geophys. Res, 102*, 17713-17727, 1997.

Grapes, R.H., Uplift and exhumation of alpine schists, Southern Alps, New Zealand, : thermobarometric constrains, *NZ Geol. Geophys*., 38, 525-533, 1995.

Halim, N., V. Kravchinsky, S. Gilder, J.P. Cogné, M. Alexyutin, A. Sorokin, V. Courtillot and Y. Chen, A palaeomagnetic study of the Mongol-Okhotsk region : rotated Early Cretaceous volcanics and remagnetized Mesozoic sediments, *Earth, Planet. Sci. Lett.*, 159, 133-145, 1998.

Hames, W.E., and S.A. Bowring, An empirical evaluation of the argon diffusion geometry in muscovite, *Earth Plane.y Sc.e Lett., 124*, 161-169, 1994.

Harris, N.B.W., X. Ronhua, C.L. Lewis, C.J. Hawkesworth, and Z. Yuquan, Isotope geochemistry of the 1985 Tibet geotraverse, Lhassa to Golmud, in *The geological evolution of Tibet, Phil. Trans. of the Roy. Soc. London, A 327*, 263-286, 1988.

Harrison, T.M., I. Duncan, and I. McDougall, Diffusion of ^{40}Ar in biotite: temperature, pressure and compositional effect,

Geochim. Cosmochim. Acta, 49, 2461-2468, 1985.

Jiao, Sh. P., Y. F. Zhang, Sh. X. Yi, Ch. X. Ai, Y. N. Zhao, H. D. Wang, J.E. Xu, J. Q. Hu, and T. Y. Guo (1988) Geological map of Qinghai-Xizang (Tibet) plateau and adjacent areas, , scale 1:1,500,000, Liu, Z. Q., editors *Geological Publishing House*, Beijing, 1988.

Khramov, A.N, Palaeomagnetic correlation of sediment formations, *Godtechizdat*, Leningrad, 218pp, 1958

Kidd, W.S.F., and P. Molnar, Quaternary and active faulting observed on the 1985 Academia Sinica-Royal Society Geotraverse of Tibet, in *The geological evolution of Tibet, Phil. Trans. of the Roy. Soc. London, A 327*, 337-363, 1988.

Krogh, T.E., A loss contamination decomposition of zircon and extraction of U and Pb for isotopic age determination, *Geochim. Cosmochim. Act,a* 37, 485-494, 1973.

Krogh, T.E., Improved accuracy of U-Pb zircon ages by the creation of more concordant systems using air abrasion technique, *Geochim. Cosmochim. Acta*, 46, 637-649, 1982.

Lachenbruch,A.H., and J.H. Sass, Heat flow and energetics of the San Andreas fault zone, *J. Geophys. Res*, 85, 6185-6222, 1980.

Leloup, P.H., T.M. Harrison, F.J. Ryerson, W. Chen, Q. Li, P. Tapponnier nd R. Lacassin, Structural, petrological and thermal evolution of a Tertiary ductile strike-slip shear zone, Diancang Shan, Yunnan. *J. of Geophys. Res., 98*, 6715-6743, 1993.

Leloup, Ph. H., Y. Ricard, J. Battaglia and R. Lacassin, Shear heating in continental strike-slip shear zones : model and field examples, *Geophys. J. Int*, in press, 1998

Lewis C.L.E., Petrogenesis and thermal history of the Kunlun Batholith, northern Tibet. *PhD* Open University, England, 278p, 1989.

Lister, G.S. and S.L. Baldwin, Modelling the effect of arbitrary P-T-t histories on argon diffusion in minerals using the MacArgon program for the Apple Macintosh, *Tectonophysics, 253*, 83-109. 1996.

Liu, Q., J.-P. Avouac, P. Tapponnier, and Q. Zhang , Holocene movement along the southern part of the Karakoram fault, paper presented at the International Symposium on the Karakoram and Kunlun Mountains, Chin. Acad. of Sci., Xianjiang, China, June 5-9, 1992.

Lovera O.M., F.M. Richter, and T.M. Harrison, The $^{40}Ar/^{39}Ar$ thermochronometry for slowly cooled samples having a distribution of diffusion domain sizes. *J. Geophys. Res., 94*, 17917-17935, 1989.

Lovera, O.M., F.M. Richter, and T.M. Harrison, Diffusion domains determined by ^{39}Ar released during step heating, *J. geophys. Res., 96*, 2057-2069, 1991

Ludwig, K.R., Isoplot 200, a plotting and regression program for isotope geochemist, for use with HP series 200 computers, *U.S. Geol. Surv. Open-file report*, 85-513, 1987.

Maluski H. and O.A. Schaeffer, ^{39}Ar-^{40}Ar laser probe dating of terrestrial rocks, *Earth Planet. Sci. Lett., 59*, 21-27, 1982.

Matte, Ph., P. Tapponnier, N. Arnaud., L. Boujot, J.P. Avouac, Ph. Vidal., L. Qing, P. Yusheng and Y. Wang. Tectonics of western Tibet, between the Tarim and the Indus. *Earth Planet. Sci. Lett., 142*, 311-330, 1996

Mattern, F., W. Schneider, Y. Li, and X. Li, A traverse through the western Kunlun (Xinjiang, China): tentavive geodynamic implications for the Paleozoic and Mesozoic, *Geol. Runsch, 85*, 805-822, 1996.

Meyer, B., P. Tapponnier, L. Bourjot, F. Métivier, Y. Gaudemer, G. Peltzer, S. Guo, and Z. Chen, Crustal thickening in Gansu-Qinghai, lithospheric mantle subduction, and oblique, strike –slip controlled growth of the Tibet Plateau, *Geophys. J. In.t*, 135, 1-47, 1998.

Meyer, B., P. Tapponnier, Y. Gaudemer, G. Peltzer, S. Guo, and Z. Chen, Rate of left-lateral movement along the easternmost segment of the Altyn-Tagh fault, east of 96°E (China), *Geophys. J. In.t*, 124, 29-44, 1996.

Mock, C., N.O. Arnaud and J. M. Cantagrel, An early unroofing in eastern Kunlun revealed by $^{40}Ar/^{39}Ar$ thermochronology. *Earth Planet. Sci. Lett.* submitted.

Murphy M.A., A. Yin, T.M. Harrison, S.B. Durr and Z.L Chen, Stratigraphic and structural development of the Mesozoic (?) Gugu La thrust system, south-central Tibet. Geological Society of America annual meeting, *abstracts with Programs*, Geological Society of America. 27, 6, 335 pp., 1995.

Parsons I., D.C. Rex, P. Guise, and A.N. Halliday, Argon-loss by alkali feldspars. *Geochim. Cosmochim. Acta 52*, 1097-1112, 1988.

Peltzer, G. and F. Saucier, Present-day kinematics of Asia derived from geologic fault rates, *J. Geophys. Res.*, 101, 27943-27956, 1996.

Peltzer, G., and P. Tapponnier, Formation and evolution of strike-slip faults, rifts, and basins during India-asia collision : an experimental approach. *J. Geophys. Res.*, 93, 15085-15172, 1988

Peltzer, G., P. Tapponnier, Y. Gaudemer, B. Meyer, S. Guo, K. Yin, C. Chen and H. Dai, Offsets of late quaternary morphology, rate of slip and recurrence of large earthquakes on the Chang Ma fault. *J. Geophys. Res*, 93: 7793-7812, 1988.

Ritts, B.D., and U. Biffi, Magnitude of post-Middle Jurassic (Bajocian) displacement on the central Altyn Tagh fault system, Northwest China, Geological Society of America Bulletin, 112 (no.1), pp.61-74, 2000.

Roddick J.C., R.A. Cliff, and D.C. Rex, The evolution of excess argon in alpine biotites - a $^{40}Ar/^{39}Ar$ analysis. *Earth Planet. Sci. Lett.*, *48*, 185-208, 1980.

Ruffet, G., G. Feraud, and M. Amouric, Comparison of $^{40}Ar/^{39}Ar$ conventional and laser dating of biotites from the North Trégor batholith, *Geochem. Cosmochim. Acta*, *55*, 1675-1688, 1991.

Schärer, U., Z. Lian-Sheng and P. Tapponnier, Duration of strike-slip movement in large shear zones: the Red River belt, China, *Earth Planet. Sci. Lett.* 126: 379-397, 1990.

Scholz, C.H., J. Beavan, T.C. Hanks, Frictional metamorphism, argon depletion, and tectonic stress on the Alpine fault, New Zealand, J. Geophys. Res., 84, 6770-6782, 1979.

Scholz, C.H., Shear heating and the state of stress on faults, J. Geophys. Res., 85, 6174-6184, 1980.

Searle, M.P., Geological evidence against large-scale pre-Holocene offsets along the Karakoram fault: Implications for the limited extrusion of the Tibetan Plateau, *Tectonics, 15*,1, 171-186, 1996.

Stacey, J.S., and J.D., Kramers, Approximation of terrestrial lead isotope evolution by a two stage model, *Earth Planet. Sci. Lett.*, 26, 207-221, 1975.

Steiger, R.H., and E. Jäger, Subcommission on geochronology : convention on the use of decay constants in geo- and cosmochronology, *Earth Planet. Sci. Lett.*, 36, 359-362, 1977.

Tapponnier, P., and P. Molnar P, Active faulting and tectonics of China, *J. Geophys. Re*s., 2905-2930, 1977.

Tapponnier, P., G. Peltzer and R. Armijo, On the mechanics of the collision between India and Asia. In: Collision Tectonics, Coward and Ries (eds), *Geological Society of London special publication, 19*, 115-157, 1986.

Tapponnier, P., Mechanisms of "extensional or denudation" faulting in regions of crustal shortening : an updated overview. In : Late Orogenic extension in Mountain Belts, Malavieille and Seranne (eds), Int. Meet. 4-6, Montpellier, *Ed. BRGM*, *21*, p.192, 1993.

Thatcher, W., and Ph. England, Ductile shear zones beneath strike-slip faults : implications for the mechanics of the San Andreas fault zone, *J. Geophys. Res*., 103, 891-905, 1998.

The Royal Society, The geological evolution of Tibet, Phil. Trans. of the Roy. Soc. London, A 327, 1-413, 1988

Van der Woerd, J., F.J. Ryerson, P. Tapponnier, Y . Gaudemer, R. Finkel, A.S. Mériaux, M. Caffee, Z. Guoguang and H. Qunlu, Holocene left-slip rate determined by cosmogenic surface dating on the Xidatan segment of the Kunlun fault (Qinghai, China), *Geology*, 26,8 695-698, 1998.

Wetherill G. W., Discordant uranium lead ages. *Trans. Am. Geoph. Union 37*, 320-326, 1956.

White, S.H., The effect of strain on the microstructures, fabrics, and deformation mechanisms in quartzites. P*hilosophical Transactions of the Royal Society of London, Ser. A., v. 283,* p. 69-86, 1976.

Xu, R., U. Schärer, and C.J. Allègre, Magmatism and metamorphism in the Lhassa block (Tibet): a geochronological study, *J. of Geology*, *93*, 41-57, 1985.

Xu, R., Z. Yuquan, X. Yingwen, Ph. Vidal, N. Arnaud, Z. Qiaoda, and Z. Dunmin, Isotopic geochemistry of plutonic roks, in Geological evolution of the Karakoram and Kunlun mountains, P. Yusheng ed., *Seismologic Press*, 137-186, 1996.

Yin, A., and S. Nie, A phanerozoic palinspastic reconstruction of China and its neighbouring regions, in *Tectonic evolution of Asia*, edited by A. Yin, and T.M. Harrison, 442-485, Cambridge University Press, Cambridge, 1996.

Yin A, M.A. Murphy-M-A; T.M Harrison-T-M; S.B. Durr, Z. Chen,; X. Wang, X. Zhou-X, F.J. Ryerson-F-J, W.S.F. Kidd Significant crustal shortening in the Lhasa Block (southern Tibet) predates the Indo-Asian collision. Geological Society of America annual meeting, *abstracts with Programs*, Geological Society of America. 27, 6, p. 335, 1995.

Yuquan, Z., X. Yingwen, X. Ronghua, Ph. Vidal and N. Arnaud Geochemistry of granitoids rocks, in Geological evolution of the Karakoram and Kunlun mountains, P. Yusheng ed., *Seismological press*, Beijing, China, 94-123, 1996

Captions of tables.

Table 1: results of U/Pb dating.

Table 2: results of Rb/Sr dating. The maximum error in $^{87}Rb/^{86}Sr$ is systematically ±2%. $^{87}Sr/^{86}Sr$ has been normalized to $^{86}Sr/^{88}Sr=0.1194$, with errors at 2σ which refer to the last digit.

Table 3: Results $^{40}Ar/^{39}Ar$ dating by step heating analysis. For micas the table gives isotopic data errors and age, with the experimental ^{39}Ar moles released and cumulative $\%^{39}Ar$. ratios are corrected for blanks, analytical deviations and neutron interference reactions only. For the K-feldspars, an additional table is provided, which gives diffusion parameters calculated during heating, with the inverse of absolute temperature (1000/T), and diffusion data for each step. Also shown are E and $\log(D_o/r_o^2)$ obtained by linear regression on arrhenius plots with associated errors.

Captions of figures.

Figure 1: Sketch map of active tectonic features associated to the Indian collision in Asia. Classical patterns for faults have been used. Small dashed open squares show the locations of detailed geological maps of figure 2 and 4. Inset shows a schematic terrane map of Asia from Yin and Nie [1996] modified.

Figure 2: Geological sketch map of eastern Kunlun along the Xidatan valley. The map is adapted from the chinese 1:1500000 Geological map (Liu, Z. Q., editor, 1988 modified **,** the Royal Society geotraverse observations and personal observations. Samples numbers are shown with their complete names.

Figure 3: Field and micro photographs of orthogneisses from the Xidatan segment of the Kunlun fault. A-B: field view of the deformation on planes roughly perpendicular to the foliation (S1 on photo A), with dip of the foliation toward reader (dashed arrow); C: close photograph of augen feldspars showing sinistral shear planes; D: microphotograph in transmitted natural light showing deformed magmatic muscovites underlying sinistral shear; E-F: microphotograph in polarized light showing fractured and rotated magmatic microcline, and recrystalized quartz.

Figure 4: Geological sketch map of western Kunlun along the Karakax valley. The map is adapted from Matte et al., 1996. Samples numbers are shown without the prefix "K89G" that should be added to every sample to be compared with text and other figures.

Figure 5: U/Pb dating of sample QGS 17 from Xidatan valley.

Figure 6: Rb/Sr dating of a/ sample QGS 17 and b/ sample QGS 16 from Xidatan valley. Data from various minerals are indicated on the isochrones as follows: Ms: muscovite, Bt: biotite, Fd: feldspar, WR: whole rock. Number in parenthesis behind initial ratio shows error on the last digit of the ratio.

Figure 7: $^{40}Ar/^{39}Ar$ age spectrum from micas in Xidatan. The plateau age is given at 1σ and includes error on J factor. It is indicated with the corresponding steps used in its calculation.. TF age is the total fusion age. Lettering refers to the type of mineral dated, muscovites, biotites.

Figure 8a and b: $^{40}Ar/^{39}Ar$ age spectrum from micas in the Karakax valley. Same conventions apply as in figure 7. When age spectra are complex $^{39}Ar_K/^{37}Ar_{Ca}$ and $^{38}Ar_{Cl}/^{39}Ar_K$ are shown as proxies for K/Ca and Cl/K ratios. They are discussed in the text to derive the most meaningful ages.

Figure 9: Model of argon loss calculated for Xidatan mica samples following several kinetic parameters solutions. The three sets of lines indicate equal argon loss models for various sets of diffusion data and various values of argon losses. The dashed box shows the range of temperatures for a plausible heating event lasting for 5-10 Ma.

Figure 10a and b: Cooling histories modeled on K-feldspars from Xidatan valley gneisses using the multi-domain theory of Lovera et al. (1989, 1991). A: age spectra; B: diffusion data with laboratory heating schedule as inset; C: resulting cooling model. In A and B experimental data curve is thin while model is bold. Data from micas and apatite (fission tracks from *Lewis*, [1989]) are shown as a confirmation of the model consistency for sample K93G36. Unsupported part at the end

of thermal model for K93G30 is shown as dashed (see text for details). Both models suggest a significant change in cooling rate at ca 25-28 Ma.

Figure 11: Model of argon loss in the micas from Karakax gneisses. Two hypothesis allow modeling: A/ thermal disturbance at ca 300°C lasting 5 to 15 Ma, or B/ slow cooling from 300°C to 250°C between 120 Ma and 80 Ma.

Figure 12: Cooling histories modeled on K-feldspars from the Karakax valley using the multi-domain theory. Same rules as in figure 10. Both feldspars are almost certainly affected by excess argon and thus yield only crude trivial model. They nevertheless indicate a significant Cenozoic thermal disturbance or very slow cooling.

Xidatan Orthogneiss (QGS 17) [a]	Weight (mg)	Concentrations (ppm)		$^{206}Pb/^{204}Pb$ measured	Atomic ratios [b]			Apparent ages (Ma) [b]		
		U	Pb		$^{206}Pb^*/^{238}U$	$^{207}Pb^*/^{235}U$	$^{207}Pb^*/^{206}Pb^*$	$^{206}Pb^*/^{238}U$	$^{207}Pb^*/^{235}U$	$^{207}Pb^*/^{206}Pb^*$
Zircons										
1- Ab, small, needles, Inc, Trp	0.0594	476	28.0	1252	0.06105	0.45838	0.05445	382	383	390
2- Ab, small, needles, Inc, Trp	0.1006	526	31.7	3151	0.06282	0.47477	0.05481	393	394	404
3- Ab, small, Inc, Trp	0.0775	729	44.6	2885	0.06343	0.51585	0.05898	396	422	567
4- Nab, medium,needles, Inc, Trp	0.1074	706	40.7	3544	0.06402	0.51136	0.05793	400	419	527
6- Ab, medium, Inc, Trp	0.1006	709	41.0	3513	0.06081	0.46211	0.05511	380	386	417
5- Ab, medium, Inc, Trp, Rd	0.1021	658	39.6	2086	0.06297	0.48728	0.05361	394	403	467
7- Ab, large, Inc, Trp, Rd	0.0593	583	42.1	2511	0.07228	0.79069	0.07933	450	591	1180
8- Ab, large, Inc, Trp, Rd	0.0631	664	73.6	4317	0.11025	1.58109	0.10401	674	963	1697

[a]: The individual analyses were performed on euhedral, unbroken, crack-free from the best quality grains of the population

Small = grains 50-100 µm in long ; medium = 100 -150 µm in long ; large > 150 µm in long ; Nab = no abraded ; Ab = Abraded , Rd = rounded, Inc = colorless and Trp = transparent.

[b]: Ratio corrected for mass discrimination (± 0.1%/amu for Pb and U), spike contribution, 15 pg of Pb blank, 1 pg of U blank and initial common Pb as determined determined from Stacey and Kramers (1975) at 384 Ma.

* : radiogenic.

Table 1

Sample :		Rb (ppm)	Sr (ppm)	$^{87}Rb/^{86}Sr$ [a]	$^{87}Sr/^{86}Sr$ (±2?) [b]
Deformed pegmatite (QGS 16)					
Feldspar		176	33.3	15.5	0.75690 ± 7
Muscovite 1	(300/400 ?m)	628	3.10	713	2.78701 ± 50
Muscovite 2	(400/600 ?m)	680	2.25	1151	3.79145 ±35
Muscovite 3	(600/800 ?m)	593	1.77	1324	4.31030 ± 80
Muscovite 4	(> 800?? m)	583	1.12	1826	5.72020 ± 30
Orthogneiss (QGS 17)					
Whole Rock		177	60.9	8.57	0.751365 ± 4
Feldspar		177	130	4.02	0.74246 ± 4
Muscovite 1	(300/400 ?m)	535	24.9	63.8	0.89389 ± 4
Muscovite 2	(400/600 ?m)	505	30.2	49.7	0.87593 ± 4
Muscovite 3	(600/800 ?m)	526	24.0	65.48	0.92148 ± 33
Biotite 1	(200/300 ?m)	1040	52.9	58.21	0.84173 ± 5
Biotite 2	(300/400 ?m)	539	13.4	120	0.91101 ± 5
Biotite 3	(400/600 ?m)	997	9.51	323	1.24120 ± 9

a : The maximum error for ($^{87}Rb/^{86}Sr$) is ??2 %
b : Normalized for ($^{86}Sr/^{88}Sr$) = 0.1194

Table 2

Temp °C	$^{40}Ar/^{39}Ar$	$^{37}Ar/^{39}Ar$	$^{36}Ar/^{39}Ar$ (10^{-3})	^{39}Ar (10^{-14}moles)	$F^{39}Ar$ released	$\%^{40}Ar^*$	$^{40}Ar^*/^{39}Ar$	Age Ma	± 1σ Ma
K93G30	Muscovite		J=0 .0006724		wt= 4.9 mg				
500	53.871	0.067	38.643	0.044	2.11	73.11	42.67	50.88	1.72
600	87.957	0.045	11.940	0.105	7.11	91.88	84.50	99.19	3.36
700	98.391	0.025	6.312	0.198	16.56	95.01	96.57	112.85	3.56
800	103.008	0.009	4.293	0.543	42.55	96.80	101.76	118.69	5.05
850	101.856	0.016	2.172	0.343	58.95	93.92	101.23	118.10	4.35
900	103.574	0.018	2.421	0.270	71.84	89.92	102.88	119.94	4.92
950	104.661	0.024	2.095	0.187	80.80	83.28	104.06	121.27	4.45
1000	106.763	0.034	1.478	0.246	92.55	84.50	106.34	123.83	4.29
1100	109.987	0.140	0.000	0.156	100.00	53.70	110.02	127.93	3.19

Temp °C	$^{40}Ar/^{39}Ar$	$^{37}Ar/^{39}Ar$	$^{36}Ar/^{39}Ar$ (10^{-3})	^{39}Ar (10^{-16}moles)	$F^{39}Ar$ released	$\%^{40}Ar^*$	$^{40}Ar^*/^{39}Ar$	Age Ma	± 1s Ma
K93G36	Muscovite		J= .0006683		wt= 18.9 mg				
600	88.390	0.020	8.960	0.094	0.68	42.69	85.80	100.06	2.58
700	100.798	0.007	8.683	1.655	12.57	90.02	98.28	114.09	2.11
800	108.916	0.002	5.861	5.111	49.31	95.50	107.22	124.06	2.29
850	106.761	0.004	4.891	1.601	60.82	88.31	105.34	121.98	2.23
900	110.804	0.004	5.863	1.907	74.53	88.81	109.10	126.16	2.38
950	112.076	0.003	3.920	2.447	92.12	90.45	110.94	128.19	2.41
1000	113.670	0.009	1.553	1.078	99.87	80.65	113.22	130.73	2.41
1050	171.051	0.795	154.024	0.019	100.00	5.08	126.58	145.05	1.51

Temp °C	$^{40}Ar/^{39}Ar$	$^{37}Ar/^{39}Ar$	$^{36}Ar/^{39}Ar$ (10^{-3})	^{39}Ar (10^{-14}moles)	$F^{39}Ar$ released	$\%^{40}Ar^*$	$^{40}Ar^*/^{39}Ar$	Age Ma	± 1s Ma
K93G36	Biotite		J= .0006669		wt= 10 mg				
700	81.032	0.007	4.676	2.287	63.36	96.38	79.68	93.24	1.66
700	81.048	0.008	4.286	0.063	65.12	49.48	79.81	93.38	1.72
753	80.936	0.015	7.167	0.129	68.69	63.51	78.86	92.30	1.73
805	81.447	0.019	8.978	0.184	73.80	68.99	78.85	92.28	1.62
935	82.318	0.006	4.548	0.656	91.97	86.72	81.00	94.73	1.82
1017	85.517	0.014	3.737	0.263	99.24	70.79	84.44	98.63	1.82
1075	97.066	0.238	18.757	0.027	100.00	16.87	91.68	106.76	1.81

Temp °C	$^{40}Ar/^{39}Ar$	$^{37}Ar/^{39}Ar$	$^{36}Ar/^{39}Ar$ (10^{-3})	^{39}Ar (10^{-14}moles)	$F^{39}Ar$ released	$\%^{40}Ar^*$	$^{40}Ar^*/^{39}Ar$	Age Ma	± 1σ Ma
K93G37	Muscovite		J=0 .0006669		wt= 16.3 mg				
700	100.922	0.013	9.769	1.013	12.04	95.78	98.09	114.32	2.14
750	106.561	0.004	7.122	1.605	31.12	97.05	104.50	121.54	1.96
809	106.156	0.004	3.275	1.498	48.92	97.70	105.21	122.34	1.88
850	106.470	0.009	5.858	0.848	59.00	95.06	104.77	121.85	2.03
930	107.499	0.007	8.177	0.863	69.26	93.21	105.13	122.25	2.07
1000	107.707	0.005	3.286	2.189	95.28	96.71	106.76	124.08	1.88
1050	105.807	0.017	0.748	0.395	99.97	82.53	105.59	122.77	1.80
1400	69.684	2.484	0.000	0.002	100.00	0.56	70.15	82.48	2.05

Temp °C	$^{40}Ar/^{39}Ar$	$^{37}Ar/^{39}Ar$	$^{36}Ar/^{39}Ar$ (10^{-3})	^{39}Ar (10^{-14}moles)	$F^{39}Ar$ released	$\%^{40}Ar^*$	$^{40}Ar^*/^{39}Ar$	Age Ma	± 1σ Ma
K93G37	Biotite	J=0.0006749		wt= 10 mg					
500	78.229	0.072	39.259	0.11	3.38	63.22	66.86	79.62	1.40
600	91.666	0.000	8.553	0.44	16.27	78.80	89.19	105.45	1.59
700	96.606	0.006	3.733	0.49	30.69	91.02	95.53	112.71	2.07
800	96.939	0.000	2.459	0.64	49.56	70.39	96.23	113.51	1.74
900	95.484	0.007	4.418	0.30	58.47	83.08	94.20	111.20	1.80
950	93.343	0.000	3.065	0.38	69.56	86.19	92.45	109.20	1.78
1000	94.331	0.012	2.098	0.43	82.15	87.47	93.72	110.65	1.66
1100	100.264	0.007	1.699	0.58	99.12	85.55	99.77	117.56	1.92
1200	124.377	0.000	11.179	0.03	99.93	19.84	121.14	141.77	2.32
1400	440.475	0.000	626.684	0.00	100.00	2.65	258.74	290.36	6.62

Temp °C	$^{40}Ar/^{39}Ar$	$^{37}Ar/^{39}Ar$	$^{36}Ar/^{39}Ar$ (10^{-3})	^{39}Ar (10^{-14}moles)	$F^{39}Ar$ released	$\%^{40}Ar^*$	$^{40}Ar^*/^{39}Ar$	Age Ma	± 1σ Ma
K93G42	Muscovite		J= 0.0006669		wt= 27.5 mg				
600	110.801	0.016	53.069	0.374	6.85	75.95	95.41	111.29	2.10
650	118.876	0.003	38.408	0.032	7.45	54.60	107.74	125.18	1.56
700	112.285	0.003	24.254	0.999	25.77	91.47	105.25	122.39	2.10
725	107.244	0.001	7.866	1.187	47.55	95.70	104.96	122.06	2.04
800	106.115	0.002	9.745	0.950	64.98	94.30	103.29	120.18	1.95
825	106.907	0.003	15.501	0.367	71.72	87.54	102.41	119.19	2.97
850	107.701	0.004	21.650	0.250	76.31	81.62	101.42	118.08	2.41
875	110.527	0.004	24.355	0.203	80.03	77.66	103.46	120.38	2.10
900	111.712	0.003	26.109	0.161	82.97	72.74	104.14	121.14	2.10
950	111.426	0.003	24.825	0.287	88.23	78.85	104.23	121.23	2.29
1000	113.814	0.004	12.553	0.576	98.80	87.64	110.17	127.91	3.15
1100	116.906	0.030	2.381	0.062	99.93	31.36	116.22	134.68	2.23
1200	244.630	0.249	119.610	0.003	99.98	1.82	210.02	236.49	2.15
1400	247.642	1.031	355.651	0.001	100.00	0.38	144.77	166.28	4.35

Table 3
Arnaud et al., 2002

Temp °C	$^{40}Ar/^{39}Ar$	$^{38}Ar/^{39}Ar$	$^{37}Ar/^{39}Ar$	$^{36}Ar/^{39}Ar$ (10^{-3})	^{39}Ar (10^{-14}moles)	$F^{39}Ar$ released	$\%^{40}Ar^*$	$^{40}Ar^*/^{39}Ar$	Age Ma	± 1σ Ma
K 89G217		Muscovite	J=0.0065000							
700	8.375	0.024	0.029	3.671	0.24	2.03	83.03	7.24	82.96	0.03
800	8.784	0.022	0.010	1.454	0.33	4.83	91.56	8.31	94.93	0.04
900	10.305	0.021	0.003	0.779	2.35	24.63	96.81	10.03	113.99	3.34
950	10.269	0.021	0.001	0.317	2.75	47.86	98.19	10.14	115.11	2.99
1000	10.345	0.021	0.002	0.204	1.47	60.26	97.61	10.25	116.34	1.33
1050	10.546	0.021	0.001	0.101	1.84	75.78	98.08	10.48	118.88	0.32
1100	10.557	0.021	0.002	0.000	1.99	92.58	98.04	10.52	119.33	0.29
1200	11.083	0.020	0.005	0.118	0.70	98.52	93.01	11.01	124.71	0.29
1400	29.034	0.028	0.000	51.970	0.18	100.00	39.23	13.41	150.73	1.17

Temp °C	$^{40}Ar/^{39}Ar$	$^{38}Ar/^{39}Ar$	$^{37}Ar/^{39}Ar$	$^{36}Ar/^{39}Ar$ (10^{-3})	^{39}Ar (10^{-14}moles)	$F^{39}Ar$ released	$\%^{40}Ar^*$	$^{40}Ar^*/^{39}Ar$	Age Ma	± 1σ Ma
K89G204		Biotite	J=0.0163800		wt= 12.7 mg					
400	6.266	0.014	0.117	1.297	0.04	1.76	93.19	5.90	166.53	3.19
450	8.877	0.013	0.046	0.373	0.13	7.19	98.56	8.77	242.27	4.54
500	14.358	0.012	0.054	0.175	0.11	11.94	99.48	14.31	379.99	6.87
550	15.020	0.012	0.041	0.136	0.14	17.73	99.63	14.99	396.02	7.13
600	15.409	0.012	0.031	0.112	0.19	25.50	99.74	15.38	405.35	7.27
650	15.422	0.012	0.050	0.149	0.11	30.04	99.63	15.38	405.44	7.29
700	16.537	0.013	0.083	0.147	0.11	34.73	99.62	16.50	431.69	7.69
750	16.807	0.013	0.181	0.180	0.11	39.16	99.59	16.78	438.00	7.81
775	17.019	0.013	0.212	0.161	0.10	43.23	99.61	17.00	443.12	7.87
800	17.083	0.013	0.155	0.086	0.15	49.33	99.77	17.08	444.95	7.89
825	17.182	0.013	0.201	0.197	0.05	51.46	99.45	17.15	446.63	7.92
850	16.063	0.013	0.223	0.127	0.19	59.33	99.85	16.05	421.15	7.53
850	15.909	0.013	0.055	0.065	0.14	65.27	99.82	15.90	417.51	7.47
875	15.855	0.013	0.049	0.012	0.25	75.84	99.89	15.86	416.57	8.84
900	15.917	0.013	0.067	0.103	0.12	80.98	99.72	15.89	417.46	7.47
950	15.956	0.013	0.206	0.099	0.37	96.41	99.83	15.95	418.79	7.50
1000	16.213	0.013	3.072	1.063	0.09	100.00	99.60	16.27	426.17	7.61
1400	Fuse, no 39Ar									

Temp °C	$^{40}Ar/^{39}Ar$	$^{38}Ar/^{39}Ar$	$^{37}Ar/^{39}Ar$	$^{36}Ar/^{39}Ar$ (10^{-3})	^{39}Ar (10^{-14}moles)	$F^{39}Ar$ released	$\%^{40}Ar^*$	$^{40}Ar^*/^{39}Ar$	Age Ma	± 1σ Ma
K89G44		Muscovite	J=0.0163800		wt= 16.9 mg					
400	32.205	0.023	0.077	38.866	0.01	0.17	64.95	20.94	532.10	9.28
500	6.810	0.015	0.123	5.258	0.02	0.62	77.62	5.30	150.18	2.90
550	3.895	0.013	0.125	2.275	0.03	1.34	83.17	3.25	93.55	1.84
600	4.326	0.013	0.101	1.335	0.12	3.79	91.24	3.95	113.11	2.19
650	3.949	0.013	0.080	0.615	0.12	6.20	95.58	3.78	108.38	2.11
700	4.502	0.013	0.086	0.690	0.17	9.64	95.67	4.31	123.12	2.39
750	5.148	0.012	0.074	0.681	0.29	15.61	96.27	4.96	140.89	2.72
800	5.403	0.012	0.047	0.479	0.45	25.01	97.49	5.27	149.36	2.87
850	5.489	0.013	0.025	0.237	0.67	38.95	98.79	5.42	153.53	2.95
900	5.210	0.013	0.042	0.222	0.68	53.00	98.82	5.15	146.12	2.81
1000	5.412	0.012	0.032	0.218	1.01	73.93	98.87	5.35	151.62	2.92
1100	6.232	0.012	0.050	0.285	1.13	97.32	98.74	6.16	173.30	3.31
1200	13.372	0.012	0.714	2.138	0.13	100.00	95.81	12.84	344.28	6.27

Temp °C	$^{40}Ar/^{39}Ar$	$^{38}Ar/^{39}Ar$	$^{37}Ar/^{39}Ar$	$^{36}Ar/^{39}Ar$ (10^{-3})	^{39}Ar (10^{-14}moles)	$F^{39}Ar$ released	$\%^{40}Ar^*$	$^{40}Ar^*/^{39}Ar$	Age Ma	± 1σ Ma
K89G42		Muscovite	J=0.0163800		wt= 20.37 mg					
400	10.513	0.021	0.122	19.634	0.01	0.12	44.83	4.83	137.45	2.83
450	7.074	0.017	0.106	11.176	0.01	0.24	52.80	3.85	110.19	2.32
500	6.083	0.015	0.107	6.315	0.01	0.49	68.14	4.26	121.80	2.47
550	6.011	0.014	0.232	3.200	0.02	0.84	83.77	5.11	145.02	2.82
600	6.243	0.013	0.336	1.678	0.04	1.59	92.41	5.79	163.60	3.16
650	6.275	0.013	0.286	0.736	0.08	3.12	96.77	6.09	171.67	3.28
700	6.364	0.013	0.055	0.348	0.12	5.53	98.23	6.27	176.35	3.37
750	6.426	0.012	0.056	0.299	0.13	8.18	98.56	6.35	178.41	3.40
800	6.527	0.012	0.050	0.270	0.22	12.57	98.76	6.45	181.31	3.65
850	6.651	0.013	0.042	0.264	0.56	23.85	98.85	6.58	184.65	3.66
700	6.483	0.012	0.020	0.000	0.02	24.20	97.76	6.48	182.12	3.47
800	6.760	0.012	0.032	0.153	0.52	34.65	99.29	6.72	188.38	3.59
850	6.667	0.012	0.065	0.167	0.31	40.96	99.22	6.63	185.88	3.54
900	6.693	0.012	0.143	0.199	0.63	53.80	99.29	6.65	186.58	3.56
950	6.838	0.012	0.001	0.136	1.13	76.61	99.37	6.80	190.49	3.63
1000	6.971	0.012	0.052	0.097	0.59	88.63	99.58	6.95	194.48	3.69
1000	7.060	0.013	0.045	0.119	0.16	91.89	99.42	7.03	196.65	3.76
1050	7.174	0.024	0.096	0.141	0.28	97.57	99.39	7.14	199.64	3.80
1100	7.517	0.012	0.438	0.434	0.09	99.46	98.24	7.44	207.50	3.93
1150	7.774	0.012	3.291	2.562	0.02	99.82	91.48	7.41	206.74	3.97
1200	7.936	0.012	4.188	6.087	0.01	100.00	77.00	6.66	186.70	3.86

Temp °C	$^{40}Ar/^{39}Ar$	$^{38}Ar/^{39}Ar$	$^{37}Ar/^{39}Ar$	$^{36}Ar/^{39}Ar$ (10^{-3})	^{39}Ar (10^{-14}moles)	$F^{39}Ar$ released	$\%^{40}Ar^*$	$^{40}Ar^*/^{39}Ar$	Age Ma	± 1σ Ma
K89G42		Biotite	J=0.0163800		wt= 10.1 mg					
450	7.420	0.016	0.050	12.288	0.02	0.63	51.90	3.86	110.66	2.41
500	7.052	0.013	0.009	1.663	0.12	3.92	93.03	6.57	184.42	3.52
550	6.309	0.012	0.003	0.334	0.34	13.58	98.41	6.21	174.83	3.40
600	6.267	0.012	0.002	0.105	0.74	34.63	99.48	6.24	175.48	3.40
650	6.254	0.013	0.002	0.045	0.55	50.33	99.75	6.24	175.61	3.38
700	6.206	0.013	0.005	0.006	0.19	55.76	99.85	6.21	174.64	3.38
725	6.156	0.012	0.009	0.000	0.07	57.86	99.66	6.16	173.34	3.33
750	6.343	0.013	0.021	0.035	0.06	59.57	99.45	6.34	178.12	3.40
775	6.386	0.013	0.046	0.023	0.07	61.55	99.60	6.39	179.45	3.43
800	6.551	0.013	0.037	0.049	0.09	64.19	99.57	6.54	183.64	3.51
825	6.580	0.013	0.015	0.009	0.11	67.32	99.73	6.58	184.65	3.53
850	6.202	0.012	0.007	0.025	0.15	71.73	99.69	6.20	174.37	3.38
875	6.218	0.012	0.006	0.029	0.17	76.48	99.68	6.21	174.76	3.36
900	6.240	0.012	0.009	0.040	0.16	81.06	99.62	6.23	175.27	3.40
925	6.263	0.012	0.013	0.062	0.17	85.89	99.53	6.25	175.76	3.41
950	6.287	0.012	0.016	0.070	0.17	90.78	99.49	6.27	176.33	3.43
975	6.307	0.012	0.021	0.059	0.14	94.88	99.50	6.29	176.96	3.41
1000	6.929	0.013	0.038	0.198	0.09	97.55	98.84	6.88	192.55	3.70
1025	6.982	0.013	0.088	0.339	0.06	99.15	97.97	6.89	193.02	3.69
1050	6.372	0.013	0.224	0.000	0.02	99.75	97.84	6.40	179.80	3.53
1100	6.950	0.015	1.883	0.335	0.01	99.91	91.39	7.07	197.71	4.82
1150	7.921	0.018	2.420	1.906	0.00	99.96	70.26	7.65	212.96	11.72
1200	8.503	0.019	0.489	2.419	0.00	100.00	58.62	7.86	218.44	18.32

Table 3 cont
Arnaud et al., 2002

Temp °C	$^{40}Ar/^{39}Ar$	$^{37}Ar/^{39}Ar$	$^{36}Ar/^{39}Ar$ (10^{-3})	^{39}Ar (10^{-14}moles)	$F^{39}Ar$ released	$\%^{40}Ar^*$	$^{40}Ar^*/^{39}Ar$	Age Ma	± 1s Ma
K93G36	K-feldspar		J= 0.0006669		wt= 27.2 mg				
400	5.465	0.007	6.566	0.318	2.62	24.93	3.56	4.28	0.12
425	12.881	0.005	5.797	0.169	4.00	36.21	11.20	13.43	0.26
500	19.496	0.005	2.378	0.143	5.18	41.06	18.81	22.49	0.48
525	22.707	0.005	2.578	0.774	11.54	79.71	21.96	26.23	0.33
550	22.703	0.007	2.843	0.431	15.08	67.28	21.88	26.13	0.40
575	23.189	0.008	2.826	0.297	17.53	58.51	22.37	26.72	0.43
623	23.671	0.006	3.337	0.477	21.45	65.94	22.70	27.11	0.46
650	24.239	0.006	2.667	0.480	25.39	65.23	23.47	28.01	0.43
700	25.891	0.005	2.215	0.394	28.63	55.07	25.25	30.13	0.45
734	26.898	0.006	2.233	0.477	32.55	62.58	26.25	31.31	0.50
750	28.357	0.005	2.220	0.378	35.66	57.57	27.71	33.04	0.51
775	29.967	0.005	2.014	0.320	38.29	53.68	29.38	35.01	0.55
810	30.669	0.005	2.962	0.517	42.54	61.21	29.81	35.51	0.52
825	31.883	0.005	2.266	0.366	45.55	55.32	31.23	37.18	0.53
825	33.560	0.005	2.391	0.354	48.47	44.29	32.87	39.12	0.60
825	35.258	0.005	2.364	0.346	51.31	35.42	34.57	41.12	0.63
825	39.864	0.005	2.569	0.838	58.20	25.10	39.12	46.46	0.70
700	32.952	0.004	0.000	0.013	58.31	1.54	32.95	39.22	0.42
725	33.361	0.008	0.000	0.038	58.62	2.47	33.36	39.70	0.66
753	39.714	0.002	0.000	0.050	59.03	5.22	39.71	47.16	0.91
772	42.146	0.003	0.000	0.065	59.57	8.80	42.15	50.01	1.14
789	43.339	0.003	0.000	0.086	60.28	11.24	43.34	51.40	0.95
820	45.443	0.011	3.169	0.140	61.42	16.24	44.53	52.79	0.85
840	43.015	0.009	1.755	0.057	61.89	20.55	42.51	50.43	0.71
900	45.104	0.009	6.821	0.162	63.23	38.62	43.13	51.16	0.81
945	44.803	0.008	4.632	0.222	65.05	44.24	43.46	51.55	0.86
1000	49.039	0.011	6.230	0.447	68.72	60.15	47.23	55.95	0.99
1000	53.625	0.010	5.846	0.826	75.51	44.24	51.93	61.42	0.95
1000	59.618	0.010	5.771	0.763	81.79	29.32	57.95	68.40	1.07
874	65.933	0.010	20.946	0.064	82.31	31.08	59.86	70.62	1.23
925	56.814	0.020	0.000	0.017	82.45	7.70	56.82	67.10	1.46
950	59.796	0.005	0.000	0.028	82.68	12.25	59.80	70.55	1.40
985	61.427	0.009	3.500	0.053	83.12	20.07	60.41	71.26	1.15
1030	64.795	0.011	5.984	0.105	83.99	29.28	63.06	74.32	1.17
1072	66.645	0.013	8.822	0.237	85.94	42.91	64.09	75.51	1.23
1098	69.056	0.012	10.549	0.369	88.97	51.36	66.00	77.71	1.34
1130	70.536	0.008	10.252	0.513	93.19	56.79	67.56	79.51	1.24
1158	72.142	0.004	9.246	0.592	98.06	58.71	69.46	81.69	1.34
1210	77.621	0.003	4.748	0.189	99.61	30.88	76.24	89.48	1.55
1400	-6.790	0.009	0.000	0.047	100.00	-0.96	-6.79	0.00	0.00

Temp °C	Time min	f	D/r^2	1000/T (K^{-1})	$-\log(D/r^2)$	$\log(r/r_o)$
E=18331 cal/mol	$\log(Do/ro^2)$=-0.58/s					
400	25	2.62	3.58E-07	1.486	6.446	-0.042
425	25	4.00	4.80E-07	1.433	6.319	0.001
500	25	5.18	5.64E-07	1.294	6.249	0.244
525	25	11.54	5.57E-06	1.253	5.254	-0.172
550	25	15.08	4.94E-06	1.215	5.306	-0.070
575	25	17.53	4.17E-06	1.179	5.380	0.039
623	25	21.45	8.00E-06	1.116	5.097	0.024
650	25	25.39	9.67E-06	1.083	5.014	0.048
700	30	28.63	7.63E-06	1.028	5.117	0.211
734	25	32.55	1.26E-05	0.993	4.901	0.172
750	25	35.66	1.11E-05	0.978	4.955	0.230
775	25	38.29	1.02E-05	0.954	4.991	0.295
810	27	42.54	1.67E-05	0.923	4.778	0.250
825	25	45.55	1.39E-05	0.911	4.857	0.315
825	40	48.47	8.96E-06	0.911	5.048	0.411
825	60	51.31	6.20E-06	0.911	5.208	0.491
825	270	58.20	3.66E-06	0.911	5.437	0.605
700	105	58.31	1.56E-07	1.028	6.806	1.055
725	180	58.62	2.68E-07	1.002	6.572	0.990
753	120	59.03	5.29E-07	0.975	6.277	0.897
772	90	59.57	9.21E-07	0.957	6.036	0.812
789	90	60.28	1.24E-06	0.942	5.908	0.779
820	90	61.42	2.03E-06	0.915	5.692	0.724
840	25	61.89	3.03E-06	0.898	5.518	0.670
900	25	63.23	8.72E-06	0.853	5.059	0.533
945	25	65.05	1.22E-05	0.821	4.912	0.522
1000	25	68.72	2.57E-05	0.786	4.590	0.432
1000	100	75.51	1.28E-05	0.786	4.892	0.583
1000	200	81.79	6.46E-06	0.786	5.190	0.732
874	20	82.31	5.67E-06	0.872	5.247	0.588
925	25	82.45	1.18E-06	0.835	5.926	1.002
950	25	82.68	1.99E-06	0.818	5.702	0.924
985	25	83.12	3.82E-06	0.795	5.418	0.828
1030	25	83.99	7.57E-06	0.767	5.121	0.734
1072	25	85.94	1.04E-04	0.743	3.983	0.213
1098	25	88.97	6.57E-05	0.729	4.182	0.341
1130	25	93.19	1.30E-04	0.713	3.886	0.226
1158	25	98.06	3.39E-04	0.699	3.470	0.046
1210	25	99.61	4.35E-04	0.674	3.361	0.041

Table 3 cont

Arnaud et al., 2002

Temp °C	$^{40}Ar/^{39}Ar$	$^{38}Ar/^{39}Ar$	$^{37}Ar/^{39}Ar$	$^{36}Ar/^{39}Ar$ (10^{-3})	^{39}Ar (10^{-14}moles)	$F^{39}Ar$ released	$\%^{40}Ar^*$	$^{40}Ar^*/^{39}Ar$	Age Ma	± 1σ Ma
K93G30	K-feldspar		J=0.0006450		wt= 10 mg					
400	39.457	0.020	0.003	3.733	0.24	3.30	96.00	38.37	44.11	0.87
400	6.138	0.010	0.000	0.000	0.01	3.48	37.87	6.14	7.13	0.60
450	4.172	0.018	0.000	0.000	0.04	4.00	63.48	4.17	4.85	0.17
450	5.357	0.017	0.000	0.000	0.05	4.66	65.07	5.36	6.22	0.21
500	12.144	0.020	0.000	0.000	0.13	6.48	94.69	12.14	14.08	0.28
500	18.147	0.017	0.000	5.582	0.05	7.16	79.07	16.53	19.13	0.49
550	20.682	0.021	0.000	8.073	0.09	8.35	84.46	18.34	21.22	0.44
550	21.741	0.020	0.000	7.783	0.07	9.33	80.28	19.48	22.53	0.54
600	23.136	0.022	0.000	8.260	0.08	10.41	85.46	20.74	23.97	0.50
600	23.765	0.020	0.000	8.508	0.05	11.15	81.22	21.30	24.61	0.57
650	25.407	0.021	0.000	8.005	0.08	12.31	86.88	23.09	26.67	0.55
650	26.007	0.020	0.000	5.677	0.05	12.95	83.60	24.36	28.13	0.67
700	28.555	0.021	0.000	4.735	0.09	14.24	91.55	27.18	31.36	0.64
700	28.555	0.021	0.000	4.735	0.09	15.53	91.55	27.18	31.36	0.64
700	30.798	0.020	0.000	1.729	0.06	16.40	90.90	30.30	34.91	0.76
750	34.895	0.020	0.000	3.980	0.11	17.90	93.86	33.74	38.84	0.78
750	36.642	0.020	0.000	2.480	0.10	19.34	93.81	35.92	41.32	0.84
800	39.457	0.020	0.052	3.733	0.24	22.64	96.00	38.37	44.11	0.87
800	42.061	0.021	1.562	2.892	0.33	27.21	94.44	41.22	47.34	0.97
800	44.729	0.021	0.000	4.999	0.33	31.73	89.94	43.28	49.67	1.10
700	39.623	0.000	0.000	15.867	0.00	31.79	28.98	35.02	40.30	9.88
750	28.419	0.009	0.285	0.000	0.01	31.96	49.80	28.42	32.77	1.75
800	40.935	0.018	2.270	0.000	0.02	32.27	83.46	40.93	47.02	1.03
850	44.478	0.020	0.000	1.502	0.22	35.30	91.90	44.04	50.53	1.10
900	45.533	0.023	3.007	4.214	0.12	36.91	93.58	44.31	50.84	1.04
950	45.891	0.021	0.626	4.525	0.29	40.90	94.85	44.58	51.14	1.03
1000	47.402	0.020	0.029	5.342	0.41	46.54	94.89	45.85	52.58	1.05
1050	51.265	0.021	0.164	6.249	0.61	55.02	94.86	49.45	56.65	1.35
1100	59.358	0.022	0.000	8.250	0.70	64.73	94.41	56.97	65.10	1.33
1200	66.597	0.022	0.000	8.989	1.75	88.99	95.11	63.99	72.96	1.47
1400	81.942	0.027	0.000	31.589	0.75	99.37	86.54	72.78	82.76	1.67
1400	266.094	0.136	0.000	664.963	0.05	100.00	23.73	73.25	83.29	5.70

Temp °C	Time min	f	D/r^2	1000/T (K^{-1})	$-\log(D/r^2)$	$\log(r/r_o)$
E=47247 cal/mol		$\log(Do/ro^2)$= 6.76/s				
400	20	0.16	1.63E-09	1.486	8.787	0.105
400	30	0.35	4.31E-09	1.486	8.366	-0.106
450	20	0.89	4.37E-08	1.383	7.359	-0.079
450	30	1.56	7.21E-08	1.383	7.142	-0.187
500	20	3.45	6.17E-07	1.294	6.209	-0.192
500	30	4.14	2.31E-07	1.294	6.636	0.021
550	20	5.38	7.68E-07	1.215	6.115	0.166
550	40	6.38	3.88E-07	1.215	6.412	0.315
600	20	7.50	1.01E-06	1.145	5.994	0.465
600	30	8.27	5.31E-07	1.145	6.275	0.606
650	20	9.46	1.38E-06	1.083	5.859	0.718
650	30	10.13	5.68E-07	1.083	6.245	0.911
700	20	11.46	1.88E-06	1.028	5.726	0.939
700	20	12.79	2.11E-06	1.028	5.675	0.913
700	30	13.68	1.03E-06	1.028	5.985	1.068
750	20	15.24	2.95E-06	0.978	5.531	1.100
750	30	16.73	2.07E-06	0.978	5.683	1.177
800	20	20.12	8.19E-06	0.932	5.087	1.114
800	85	24.84	3.26E-06	0.932	5.486	1.313
800	180	29.51	1.85E-06	0.932	5.734	1.437
700	70	29.57	7.20E-08	1.028	7.143	1.647
750	60	29.74	2.22E-07	0.978	6.654	1.662
800	30	30.07	8.50E-07	0.932	6.071	1.606
850	90	33.20	2.88E-06	0.890	5.541	1.555
900	20	34.86	7.41E-06	0.853	5.130	1.545
950	25	38.98	1.59E-05	0.818	4.798	1.559
1000	25	44.80	2.55E-05	0.786	4.593	1.622
1050	25	53.55	4.51E-05	0.756	4.346	1.652
1100	25	63.59	6.15E-05	0.728	4.211	1.727
1200	30	88.63	2.66E-04	0.679	3.575	1.664
1400	25	99.35	7.72E-04	0.598	3.112	1.852

Table 3 cont

Arnaud et al., 2002

Temp °C	$^{40}Ar/^{39}Ar$	$^{37}Ar/^{39}Ar$	$^{36}Ar/^{39}Ar$ (10^{-3})	^{39}Ar (10^{-15}moles)	$F^{39}Ar$ released	$\%^{40}Ar^*$	$^{40}Ar^*/^{39}Ar$	Age Ma	± 1σ Ma
K89G204	K-feldspar		J=0.00492	wt=0.00814 g					
450	1670.000	-0.032	2118.000	0.418	0.20	62.50	1044.00	3278.00	27.30
500	347.800	-0.026	224.800	0.724	0.55	80.90	281.30	1571.00	3.40
550	111.000	0.000	23.500	2.710	1.84	93.70	104.10	748.20	2.20
600	35.460	0.031	2.877	3.890	3.71	97.40	34.59	284.50	0.50
650	22.920	0.068	3.762	5.720	6.44	94.90	21.80	184.40	0.60
700	11.130	0.039	1.220	8.240	10.40	96.40	10.75	93.30	0.30
750	9.298	0.011	0.982	8.700	14.60	96.40	8.99	78.40	0.20
800	4.443	0.004	1.124	7.690	18.20	91.40	4.09	36.10	0.10
840	4.528	0.006	0.540	6.440	21.30	95.00	4.35	38.30	0.20
840	6.046	0.000	1.653	5.370	23.90	98.90	5.54	48.70	0.20
840	9.190	0.045	0.823	6.230	26.90	92.40	8.93	77.80	0.20
840	17.380	0.003	3.741	14.900	34.00	89.60	16.25	139.30	0.30
900	31.840	0.014	2.707	3.280	35.60	97.40	31.02	257.10	0.40
950	24.480	0.004	0.948	5.470	38.20	97.50	24.18	203.50	0.30
1000	27.410	0.005	1.164	8.940	42.50	98.00	27.05	226.20	0.40
1050	31.350	0.007	0.906	14.800	49.60	98.70	31.06	257.40	0.40
1100	33.270	0.005	1.052	19.300	58.80	98.80	32.94	271.90	0.30
1100	33.370	0.001	0.760	13.600	65.30	98.60	33.13	273.30	0.60
1100	34.200	0.000	0.000	12.700	71.40	98.20	34.32	282.40	0.70
1100	35.200	0.000	0.000	13.500	77.90	96.50	35.73	293.20	0.70
1100	37.180	0.000	0.000	17.000	86.00	91.20	37.99	310.20	1.10
1150	37.740	-0.017	0.000	2.430	87.20	97.80	38.54	314.30	1.00
1200	38.070	-0.003	0.000	8.190	91.10	98.70	38.14	311.30	1.40
1500	36.450	0.000	3.128	18.400	99.90	90.70	35.51	291.50	0.80
1500	497.900	-0.205	1443.000	0.223	100.00	14.40	71.52	545.60	25.40

Temp °C	Time min	f	D/r^2	1000/T (K^{-1})	$-\log(D/r^2)$	$\log(r/r_o)$
E=42307 cal/mol		$\log(Do/ro^2)$=4.6 /s				
450	10	0.20	5.25E-09	1.383	8.280	0.045
500	10	0.55	3.40E-08	1.294	7.469	0.053
550	10	1.84	4.06E-07	1.215	6.391	-0.122
600	10	3.71	1.36E-06	1.145	5.868	-0.063
650	10	6.44	3.65E-06	1.083	5.438	0.010
700	10	10.40	8.71E-06	1.028	5.060	0.077
750	10	14.60	1.36E-05	0.978	4.866	0.211
800	10	18.20	1.58E-05	0.932	4.800	0.396
840	10	21.30	1.60E-05	0.898	4.796	0.543
840	30	23.90	5.09E-06	0.898	5.293	0.790
840	90	26.90	2.21E-06	0.898	5.656	0.972
840	822	34.00	6.93E-07	0.898	6.159	1.226
900	26	35.60	5.62E-06	0.853	5.250	0.983
950	27	38.20	9.39E-06	0.818	5.027	1.035
1000	19	42.50	2.38E-05	0.786	4.623	0.978
1050	15	49.60	5.69E-05	0.756	4.245	0.927
1100	15	58.80	8.76E-05	0.728	4.057	0.962
1100	30	65.30	4.03E-05	0.728	4.394	1.130
1100	70	71.40	1.87E-05	0.728	4.728	1.297
1100	180	77.90	9.63E-06	0.728	5.016	1.464
1100	890	86.00	3.48E-06	0.728	5.458	1.662
1150	20	87.20	2.94E-05	0.703	4.532	1.310
1200	17	91.10	1.45E-04	0.679	3.838	1.081
1500	22	99.90	1.36E-03	0.564	2.866	1.122

Table 3 cont

Arnaud et al., 2002

Temp °C	$^{40}Ar/^{39}Ar$	$^{37}Ar/^{39}Ar$	$^{36}Ar/^{39}Ar$ (10^{-3})	^{39}Ar (10^{-15}moles)	$F^{39}Ar$ released	$\%^{40}Ar^*$	$^{40}Ar^*/^{39}Ar$	Age Ma	± 1σ Ma
K89G50	K-feldspar		J=0.004911	wt=0.00825 g					
450	852.800	0.151	820.600	0.288	0.06	71.50	610.30	2500.00	13.30
500	163.400	0.051	119.400	0.444	0.16	78.30	128.10	880.60	5.50
550	47.770	0.035	21.780	1.740	0.54	86.40	41.31	333.30	1.30
600	17.000	0.057	5.287	3.070	1.21	90.50	15.42	131.70	0.40
650	12.600	0.062	3.637	7.490	2.86	91.30	11.51	99.20	0.50
700	7.929	0.043	2.722	14,000	5.93	89.60	7.11	61.90	0.10
750	5.215	0.026	1.618	29.900	12.50	90.30	4.72	41.30	0.10
800	4.733	0.029	1.165	16.800	16.20	92.30	4.37	38.30	0.10
820	4.785	0.031	1.090	7.230	17.70	92.80	4.45	39.00	0.10
840	5.872	0.031	1.114	3.880	18.60	94.00	5.53	48.30	0.20
840	5.134	0.025	0.859	5.230	19.70	94.30	4.86	42.60	0.10
840	6.275	0.023	0.839	5.390	20.90	95.40	6.01	52.50	0.20
840	7.825	0.020	0.981	4.640	21.90	95.60	7.52	65.40	0.40
750	7.987	0.017	1.107	3.580	22.70	89.20	7.64	66.50	0.20
840	10.910	0.017	1.009	3.580	23.50	96.40	10.59	91.50	0.30
870	18.650	0.022	2.532	1.800	23.90	95.70	17.89	151.90	0.90
900	20.870	0.025	1.952	2.860	24.50	97.00	20.28	171.30	0.60
950	36.050	0.029	1.922	8.270	26.30	98.30	35.46	289.70	0.80
950	17.750	0.014	1.003	5.900	27.60	98.10	17.44	148.20	0.30
1000	41.270	0.019	1.682	16.700	31.30	98.70	40.76	329.20	0.90
1050	35.240	0.015	1.469	40.100	40.10	98.60	34.79	284.50	0.90
1075	29.550	0.015	1.312	45.600	50.10	98.50	29.14	241.30	0.70
1100	26.450	0.014	1.063	32.800	57.20	98.70	26.12	217.70	0.90
1120	27.310	0.015	1.161	30.100	63.80	98.60	26.95	224.20	0.60
1120	30.620	0.014	1.243	46.900	74.10	98.60	30.23	249.70	0.90
1120	29.180	0.013	1.114	27.700	80.20	98.70	28.83	238.90	0.60
1120	30.210	0.119	0.973	30.500	86.90	98.80	29.91	247.20	0.40
1120	31.230	0.024	2.225	42.800	96.30	96.30	30.56	252.20	1.00
1170	23.700	0.051	3.357	0.207	96.30	88.00	22.59	196.60	2.20
1240	24.280	0.017	4.818	16.900	100.00	93.50	22.84	191.80	0.90

Temp °C	Time min	f	D/r^2	1000/T (K^{-1})	$-\log(D/r^2)$	$\log(r/r_o)$
E= 48658 cal/mol		$\log(Do/ro^2)$=5.29 /s				
450	11	0.06	4.76E-10	1.383	9.322	-0.041
500	10	0.16	2.85E-09	1.294	8.545	-0.049
550	17	0.54	2.07E-08	1.215	7.685	-0.058
600	12	1.21	1.29E-07	1.145	6.889	-0.066
650	11	2.86	7.96E-07	1.083	6.099	-0.073
700	11	5.93	3.21E-06	1.028	5.493	-0.080
750	14	12.50	1.13E-05	0.978	4.948	-0.070
800	12	16.20	1.15E-05	0.932	4.938	0.107
820	10	17.70	7.05E-06	0.915	5.152	0.400
840	6	18.60	6.76E-06	0.898	5.170	0.510
840	15	19.70	3.84E-06	0.898	5.416	0.581
840	30	20.90	2.10E-06	0.898	5.678	0.671
840	41	21.90	1.39E-06	0.898	5.856	0.742
750	680	22.70	6.77E-08	0.978	7.170	0.875
840	60	23.50	7.92E-07	0.898	6.101	0.818
870	12	23.90	2.04E-06	0.875	5.691	0.805
900	11	24.50	3.61E-06	0.853	5.442	0.786
950	10	26.30	1.21E-05	0.818	4.918	0.760
950	11	27.60	8.32E-06	0.818	5.080	0.780
1000	11	31.30	2.57E-05	0.786	4.591	0.763
1050	12	40.10	6.84E-05	0.756	4.165	0.759
1075	13	50.10	9.08E-05	0.742	4.042	0.772
1100	13	57.20	7.78E-05	0.728	4.109	0.776
1120	12	63.80	9.72E-05	0.718	4.012	0.782
1120	23	74.10	9.85E-05	0.718	4.007	0.817
1120	34	80.20	5.32E-05	0.718	4.274	0.890
1120	100	86.90	2.78E-05	0.718	4.555	1.091
1120	1111	96.30	7.64E-06	0.718	5.117	1.402
1170	17	96.30	4.85E-06	0.693	5.314	1.380

Table 3 cont

Arnaud et al., 2002

Temp °C	$^{40}Ar/^{39}Ar$	$^{37}Ar/^{39}Ar$	$^{36}Ar/^{39}Ar$ (10^{-3})	^{39}Ar (10^{-10}moles)	$F^{39}Ar$ released	$\%^{40}Ar^*$	$^{40}Ar^*/^{39}Ar$	Age Ma	± 1s Ma
K89G134	K-feldspar		J=0.012	wt: 0.03674 g				Ma	Ma
450	1.582	0.117	1.853	2.470	1.42	65.12	1.04	22.34	0.10
500	0.697	0.056	0.564	3.574	3.47	75.13	0.53	11.51	0.05
550	0.651	0.054	0.443	5.230	6.47	78.99	0.52	11.31	0.03
550	0.467	0.058	0.059	2.665	8.00	92.78	0.46	9.84	0.02
600	0.595	0.082	0.311	4.987	10.87	84.02	0.51	11.03	0.03
650	0.524	0.113	0.167	5.440	13.99	90.75	0.49	10.50	0.02
700	0.509	0.144	0.170	5.661	17.24	91.04	0.47	10.22	0.02
750	0.524	0.150	0.208	5.214	20.23	89.10	0.48	10.31	0.02
800	0.567	0.123	0.311	5.030	23.12	84.01	0.49	10.51	0.03
850	0.693	0.079	0.570	5.093	26.04	75.20	0.53	11.45	0.04
850	0.798	0.050	0.754	5.165	29.01	71.22	0.58	12.45	0.04
750	0.975	0.037	1.293	6.294	32.62	60.01	0.59	12.75	0.05
800	1.053	0.018	1.050	1.240	33.33	66.98	0.74	15.94	0.09
850	1.181	0.029	1.440	1.406	34.14	61.32	0.75	16.21	0.09
900	1.123	0.043	1.278	2.012	35.30	64.45	0.74	16.04	0.09
1000	1.237	0.059	1.469	10.227	41.17	64.30	0.80	17.29	0.05
1020	1.167	0.041	1.152	13.865	49.13	70.29	0.83	17.79	0.05
1050	1.099	0.033	0.816	13.791	57.04	77.48	0.86	18.48	0.06
1050	1.035	0.037	0.706	15.489	65.94	79.37	0.83	17.83	0.22
1050	1.503	0.033	0.535	58.015	99.24	89.45	1.35	28.90	0.05
950	5.256	0.417	16.347	0.901	99.76	7.43	0.40	8.58	1.28
1000	10.499	0.149	30.051	0.057	99.79	12.60	1.50	32.19	5.40
1240	200.600	0.232	696.552	0.360	100.00	-4.10	-8.34	0.00	0.00

Temp °C	Time min	f	D/r^2	1000/T (K^{-1})	$-\log(D/r^2)$	$\log(r/r_o)$
E=32160 cal/mol		$\log(Do/ro^2)$=3.02 /s				
450	15	1.42	1.75E-07	1.383	6.756	0.026
500	12	3.47	1.09E-06	1.293	5.961	-0.057
550	12	6.47	3.26E-06	1.215	5.487	-0.017
550	12	8.00	2.42E-06	1.215	5.617	0.048
600	12	10.87	5.89E-06	1.145	5.230	0.098
650	12	13.99	8.47E-06	1.083	5.072	0.238
700	12	17.24	1.11E-05	1.028	4.956	0.375
750	12	20.23	1.22E-05	0.977	4.912	0.530
800	12	23.12	1.37E-05	0.932	4.865	0.666
850	12	26.04	1.57E-05	0.890	4.805	0.782
850	30	29.01	7.12E-06	0.890	5.147	0.953
750	699	32.62	4.17E-07	0.977	6.380	1.264
800	60	33.33	1.02E-06	0.932	5.989	1.228
850	25	34.14	2.85E-06	0.890	5.545	1.152
900	12	35.30	8.75E-06	0.852	5.058	1.042
1000	12	41.17	4.90E-05	0.785	4.310	0.903
1020	14	49.13	6.72E-05	0.773	4.173	0.877
1050	12	57.04	9.17E-05	0.756	4.038	0.871
1050	12	65.94	1.19E-04	0.756	3.923	0.814
1050	120	99.24	2.16E-04	0.756	3.666	0.686
950	854	99.76	9.10E-06	0.818	5.041	1.156
1000	110	99.79	9.03E-06	0.785	5.044	1.270

Table 3 cont

Arnaud et al., 2002

Temp °C	$^{40}Ar/^{39}Ar$	$^{37}Ar/^{39}Ar$	$^{36}Ar/^{39}Ar$ (10^{-3})	^{39}Ar (10^{-14}moles)	$F^{39}Ar$ released	$\%^{40}Ar^*$	$^{40}Ar^*/^{39}Ar$	Age Ma	± 1σ Ma
K90G81	K-feldspar		J=0.012	wt= 0.01677g					
450	1.004	0.004	0.967	0.74	0.843	70.84	0.1	15.4	0.12
475	0.641	0	0.313	0.897	1.865	84.87	0.55	11.81	0.05
500	0.588	-0.031	0.053	1.051	3.062	96.23	0.57	12.28	0.04
525	0.549	0	0.082	1.254	4.491	95.06	0.52	11.32	0.03
550	0.538	-0.022	-0.022	1.492	6.192	100.4	0.54	11.71	0.03
575	0.529	-0.03	-0.162	0.931	7.252	107.85	0.57	12.38	0.07
600	0.556	-0.009	-0.021	2.056	9.595	100.66	0.56	12.1	0.02
650	0.624	0.003	0.099	3.932	14.075	95.18	0.59	12.83	0.03
700	0.531	0.008	0.043	5.772	20.652	97.59	0.52	11.21	0.02
750	0.493	0.006	0.018	7.071	28.709	98.96	0.49	10.53	0.02
800	0.489	0.002	0.005	7.561	37.325	99.62	0.49	10.53	0.02
800	0.492	-0.005	0.003	6.472	44.699	99.53	0.49	10.6	0.02
800	0.512	0.008	0.1	4.797	50.165	94.21	0.48	10.42	0.09
700	0.57	0.003	0.242	2.91	53.481	87.11	0.5	10.74	0.04
750	0.562	-0.021	0.006	0.919	54.529	98.34	0.56	12.03	0.05
800	0.613	-0.013	0.196	2.119	56.943	89.91	0.55	11.93	0.04
850	0.774	-0.075	0.168	0.626	57.656	91.41	0.72	15.42	0.07
875	0.714	-0.049	0.138	0.875	58.653	92.63	0.67	14.38	0.05
900	0.738	-23	0.239	1.258	60.086	89.39	0.66	14.32	0.04
925	0.805	-0.023	0.357	1.526	61.825	86.04	0.69	14.98	0.06
950	0.831	-0.005	0.432	1.967	64.067	84.01	0.7	15.11	0.05
1000	0.901	0.004	0.562	4.29	68.955	81.21	0.73	15.81	0.04
1050	0.934	0.003	0.585	9.961	80.305	81.13	0.76	16.35	0.04
1050	0.913	0	0.602	10.684	92.479	80.12	0.73	15.78	0.05
950	0.972	-0.005	0.86	4.705	97.84	73.27	0.71	15.39	0.04
1000	1.085	-0.13	0.484	0.339	98.227	83.16	0.93	19.92	0.15
1050	0.987	-0.047	0.378	0.367	98.645	85.71	0.87	18.69	0.12
1075	0.966	-0.107	0.113	0.387	99.086	92.92	0.92	19.81	0.12
1100	0.977	-0.103	0.255	0.444	99.593	89.06	0.89	19.15	0.08
1150	0.896	-0.19	-0.423	0.225	99.849	93.95	1	21.56	0.15
1330	3.53	-0.334	7.389	0.153	100	35.1	1.27	27.3	0.6

Temp °C	Time min	f	D/r^2	1000/T (K^{-1})	$-\log(D/r^2)$	$\log(r/r_o)$
E=40768 cal/mol	$\log(Do/ro^2)$= 7.3/s					
450	1.2	0.84	-8	1.383	7.111	0.043
475	1.2	1.87	3.02E-07	1.337	6.52	-0.046
500	1.2	3.06	6.43E-07	1.294	6.191	-0.018
525	1.2	4.49	1.18E-06	1.253	5.929	0.032
550	1.2	6.19	1.98E-06	1.215	5.703	0.088
575	1.2	7.25	1.56E-06	1.179	5.808	0.3
600	1.2	9.59	4.30E-06	1.145	5.366	0.23
650	1.2	14.08	1.16E-05	1.083	4.937	0.291
700	1.2	20.65	2.49E-05	1.028	4.604	0.373
750	1.2	28.71	4.34E-05	0.978	4.363	0.476
800	1.2	37.32	6.21E-05	0.932	4.207	0.601
800	31	44.7	2.55E-05	0.932	4.593	0.794
800	60	50.17	1.13E-05	0.932	4.946	0.971
700	825	53.48	5.45E-07	1.028	6.263	1.203
750	120	54.53	1.23E-06	0.978	5.909	1.249
800	120	56.94	2.94E-06	0.932	5.532	1.264
850	1.2	57.66	8.92E-06	0.89	5.05	1.207
875	1.2	58.65	1.27E-05	0.871	4.898	1.218
900	1.3	60.09	1.71E-05	0.853	4.766	1.234
925	1.2	61.83	2.31E-05	0.835	4.636	1.249
950	1.2	64.07	3.08E-05	0.818	4.512	1.262
1000	1.2	68.96	7.09E-05	0.786	4.149	1.224
1050	1.2	80.31	1.85E-04	0.756	3.733	1.149
1050	30	92.48	2.54E-04	0.756	3.595	1.079
950	805	97.84	1.05E-05	0.818	4.98	1.497
1000	120	98.23	1.11E-05	0.786	4.955	1.627
1050	30	98.64	6.05E-05	0.756	4.218	1.391
1075	20	99.09	1.33E-04	0.742	3.876	1.282
1100	20	99.59	2.73E-04	0.728	3.564	1.187
1150	20	99.85	3.35E-04	0.703	3.476	1.256

Table 3 cont

Arnaud et al., 2001

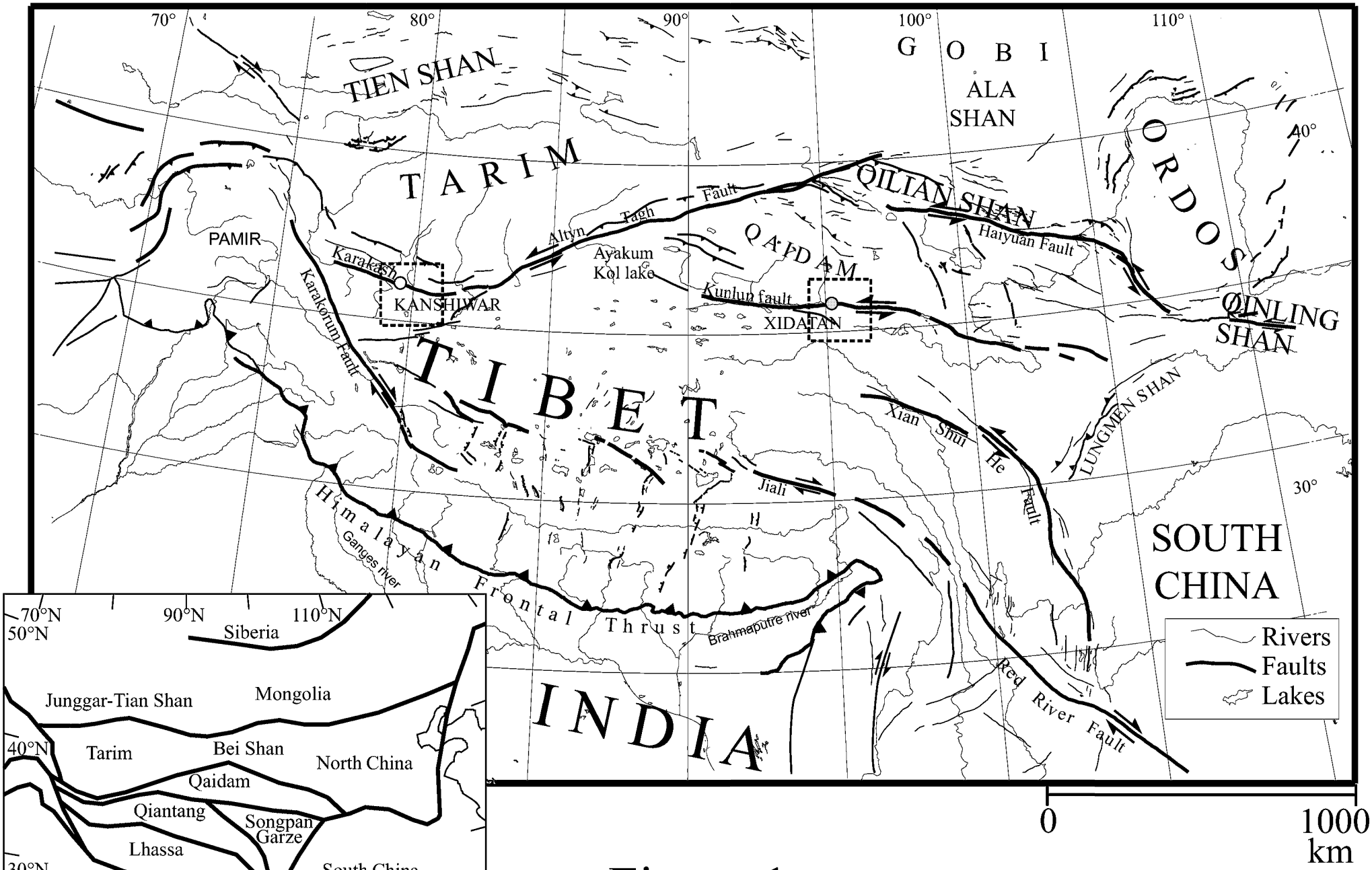

Figure 1
Arnaud et al., 2002

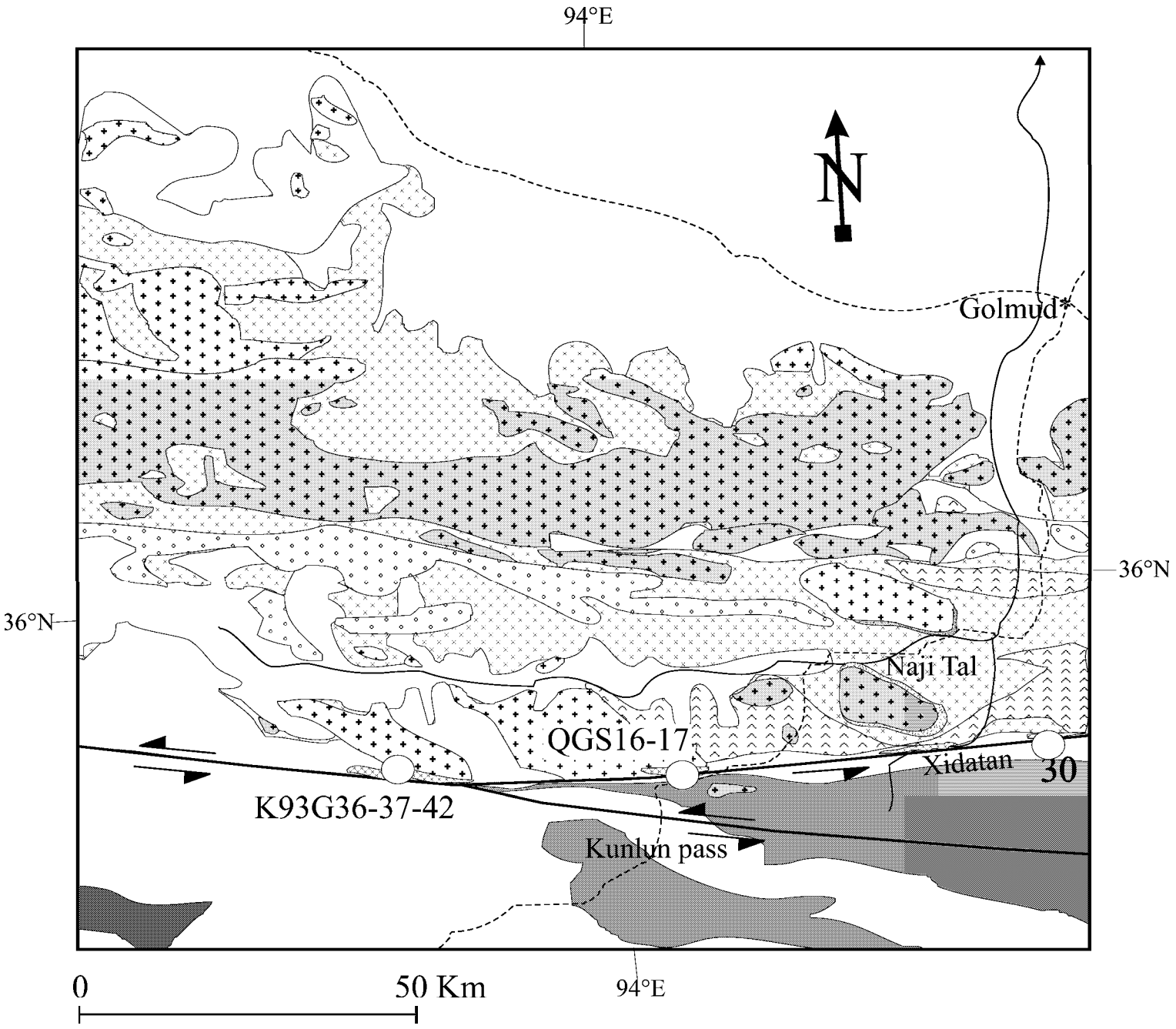

Quaternary sediments

Contact metamorphism

Mesozoic granitoids

Paleozoic granitoids

Gneisses with local metamorphic foliation

ATF: Altyn Tagh fault along its active trace

Mylonites along the Altyn-Tagh fault along the Karakax river

Triassic unconformable sandstones and conglomerates and scarce lower jurassic

Triassic slates of Bayan har affinity with loacal folding and foliation

Middle-Upper Paleozoic flyshoïd and volcanic series

Lower Paleozoic series,

Precambrian orthogneissic series,

Major fault, essentially strike-slip

Figure 2
Arnaud et al., 2002

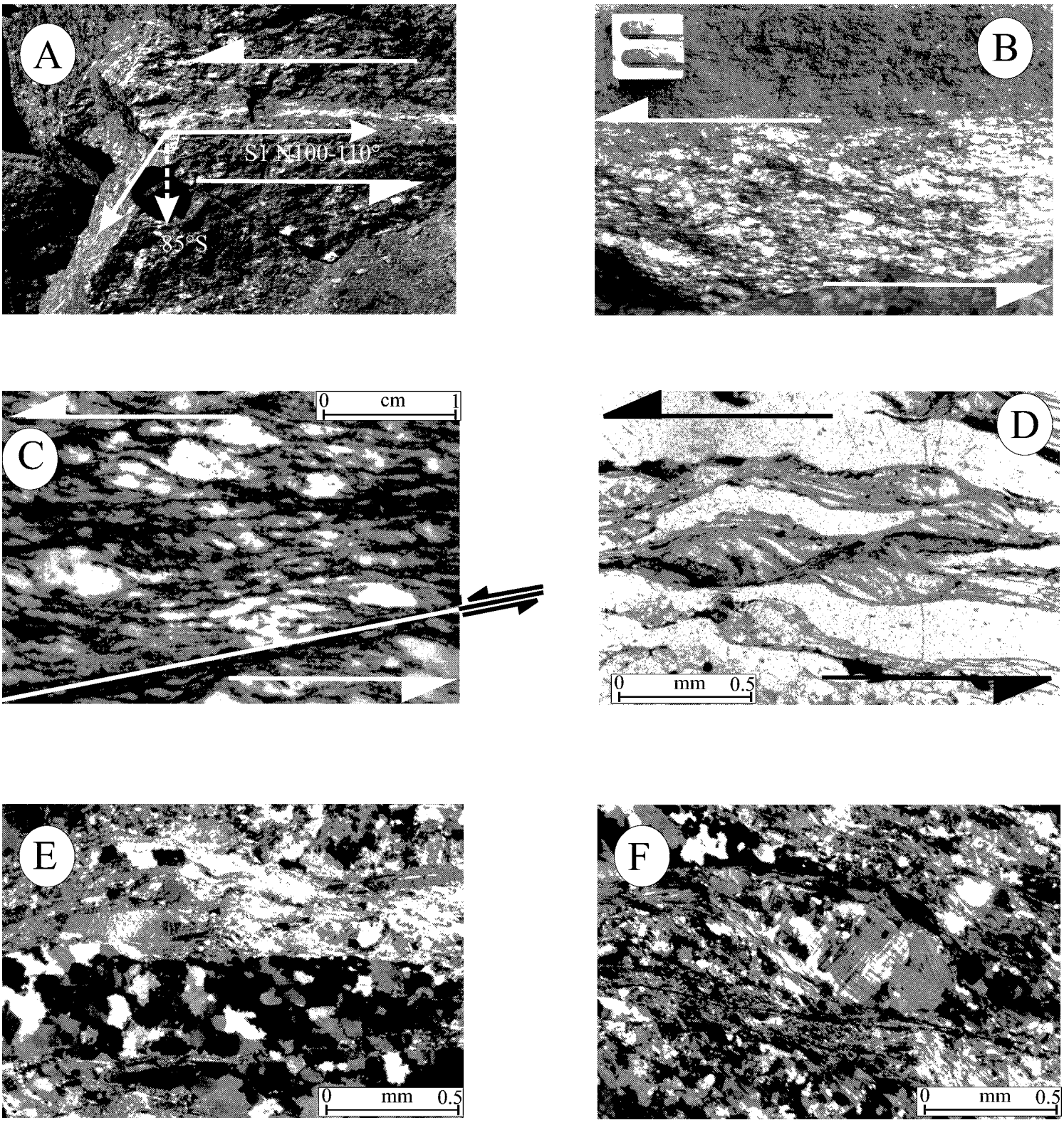

Figure 3
Arnaud et al., 2002

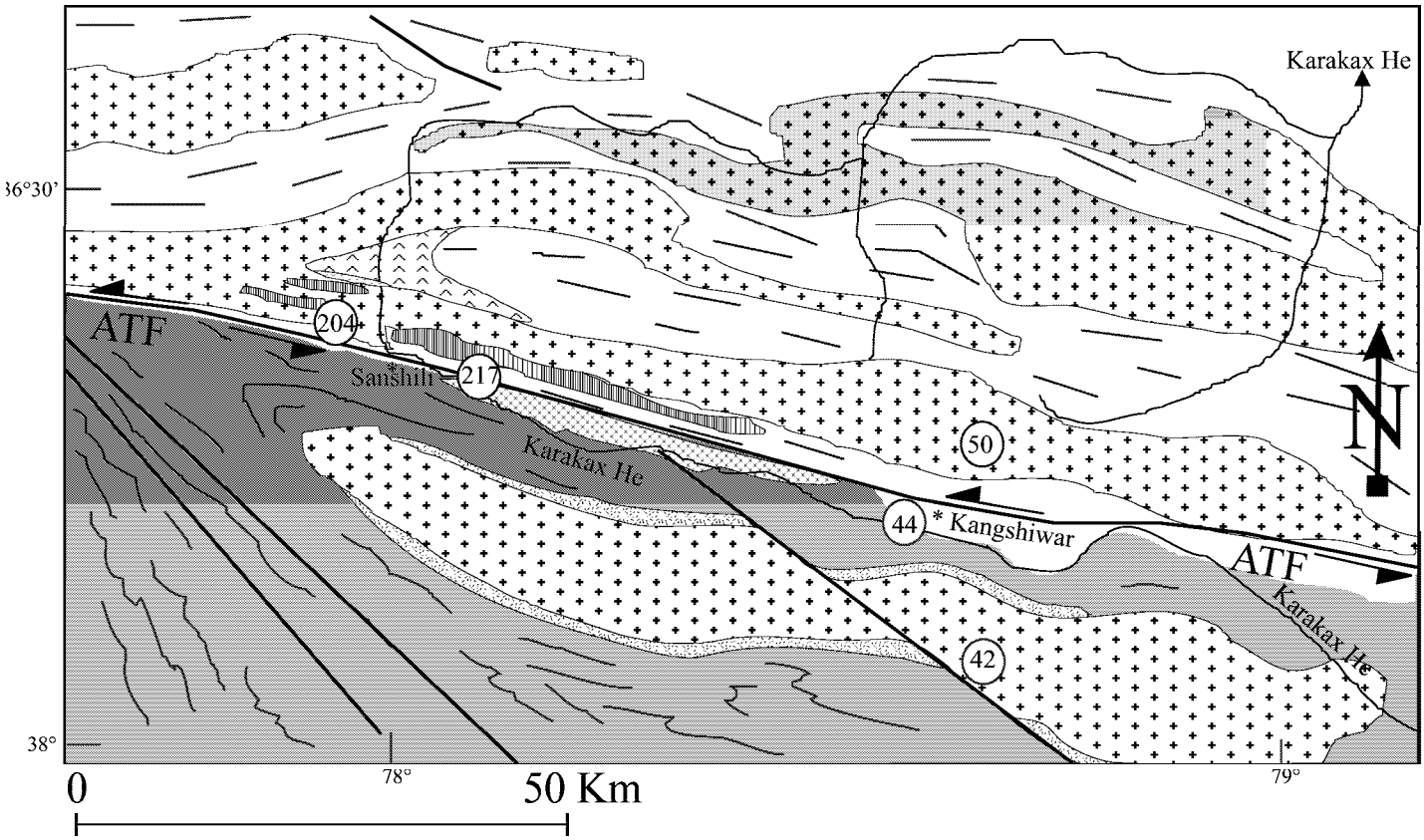

Quaternary sediments

Contact metamorphism

Mesozoic granitoids

Paleozoic granitoids

Gneisses with local metamorphic foliation

ATF: Altyn Tagh fault along its active trace

Mylonites along the Altyn-Tagh fault along the Karakax river

Jurassic detritics

Triassic slates of Bayan har affinity with local folding and foliation

Upper Paleozoic/Mesozoic mafic volcanic arc series

Upper Paleozoic acid volcanis arc series,

Major fault, essentially strike-slip

Figure 4
Arnaud et al., 2002

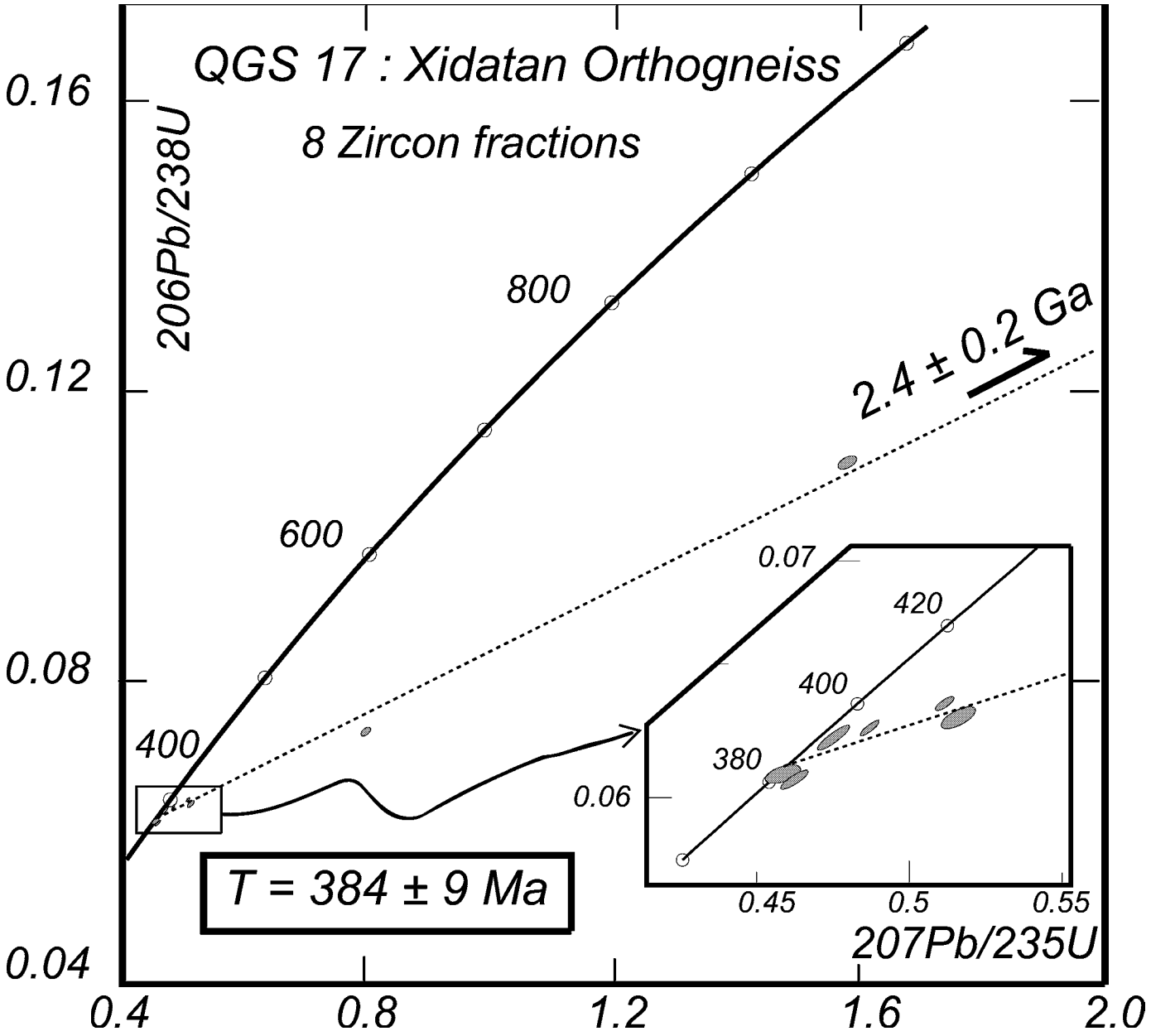

Figure 5
Arnaud et al.

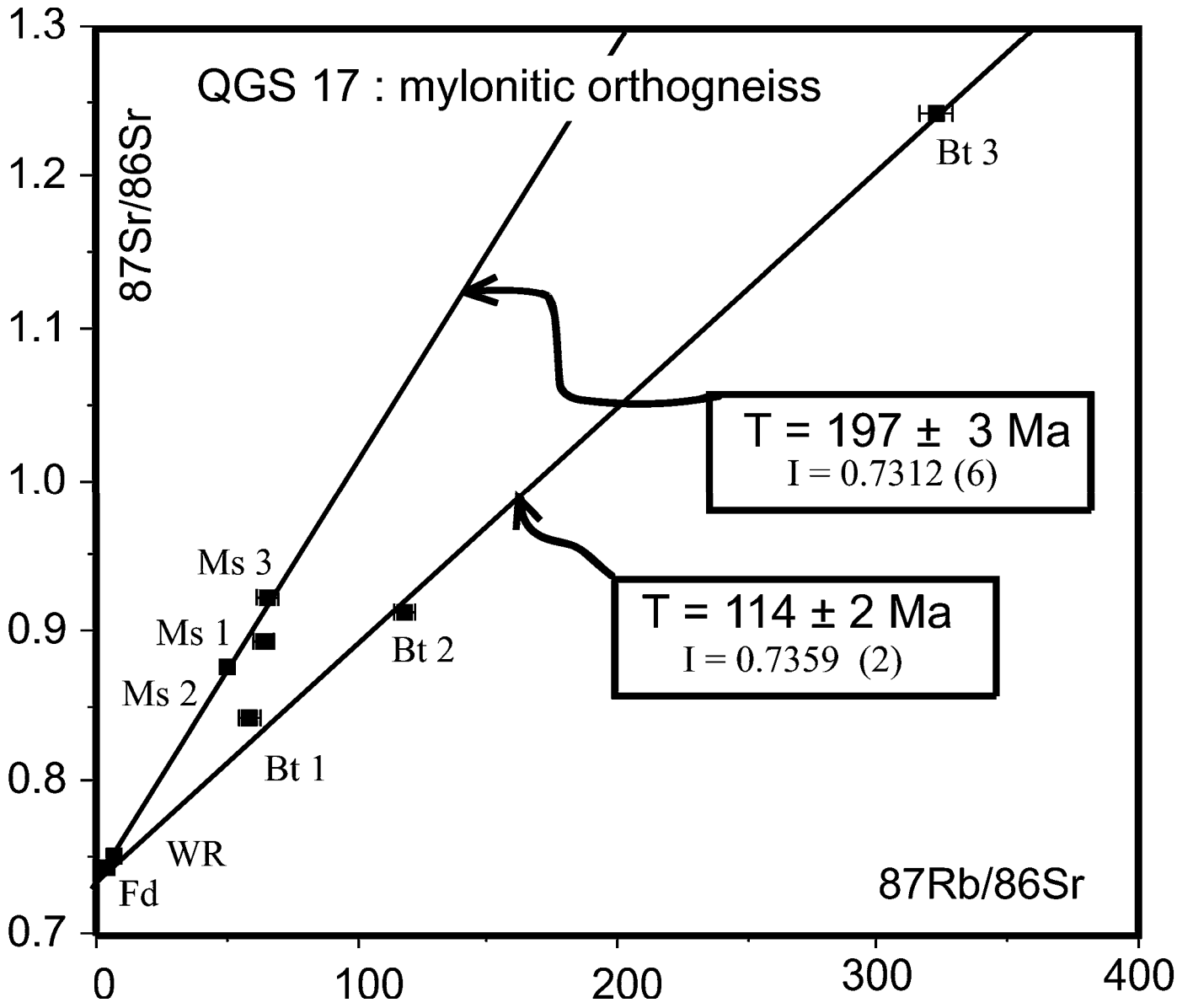

Figure 6a
Arnaud et al.

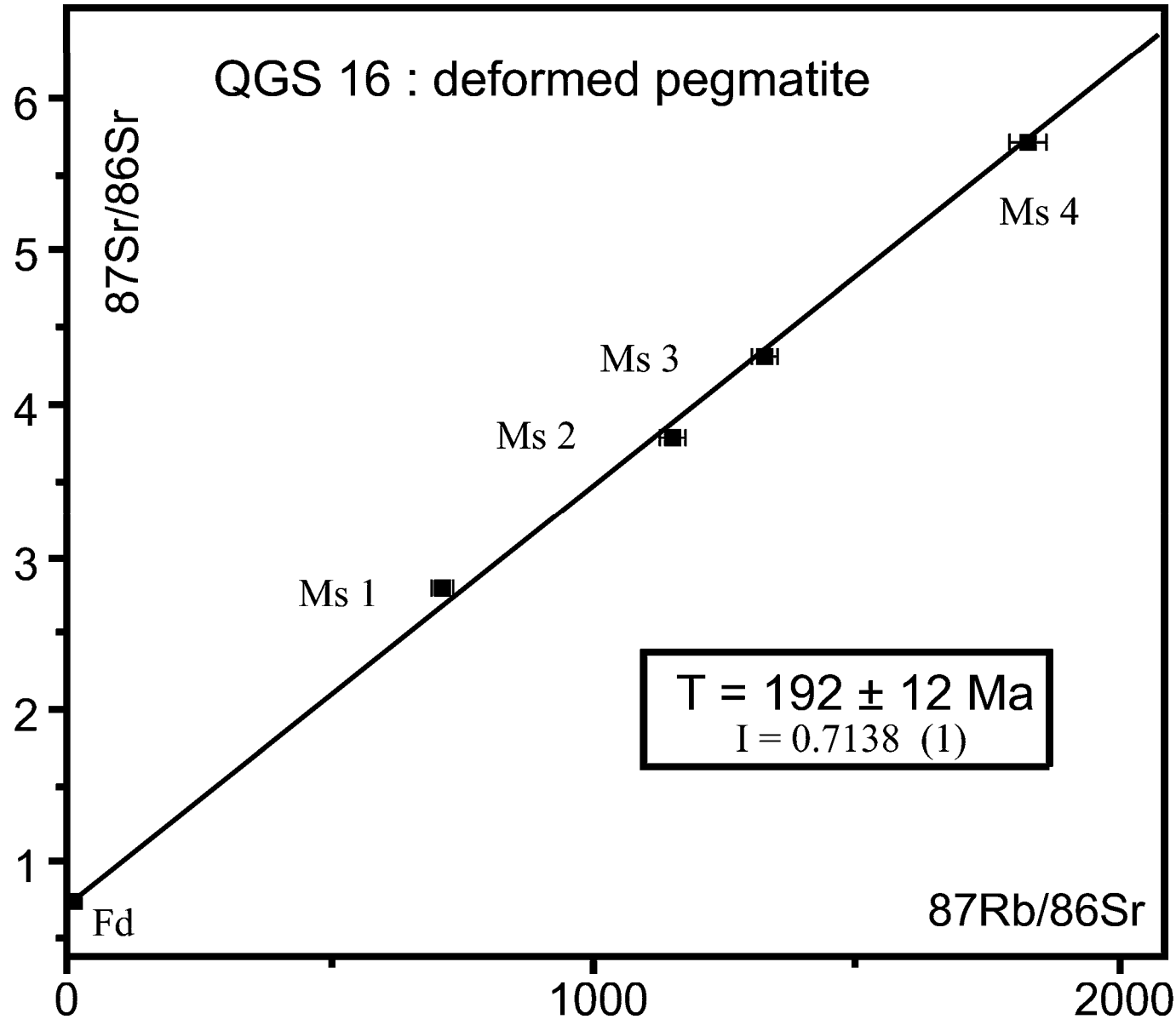

Figure 6b
Arnaud et al.

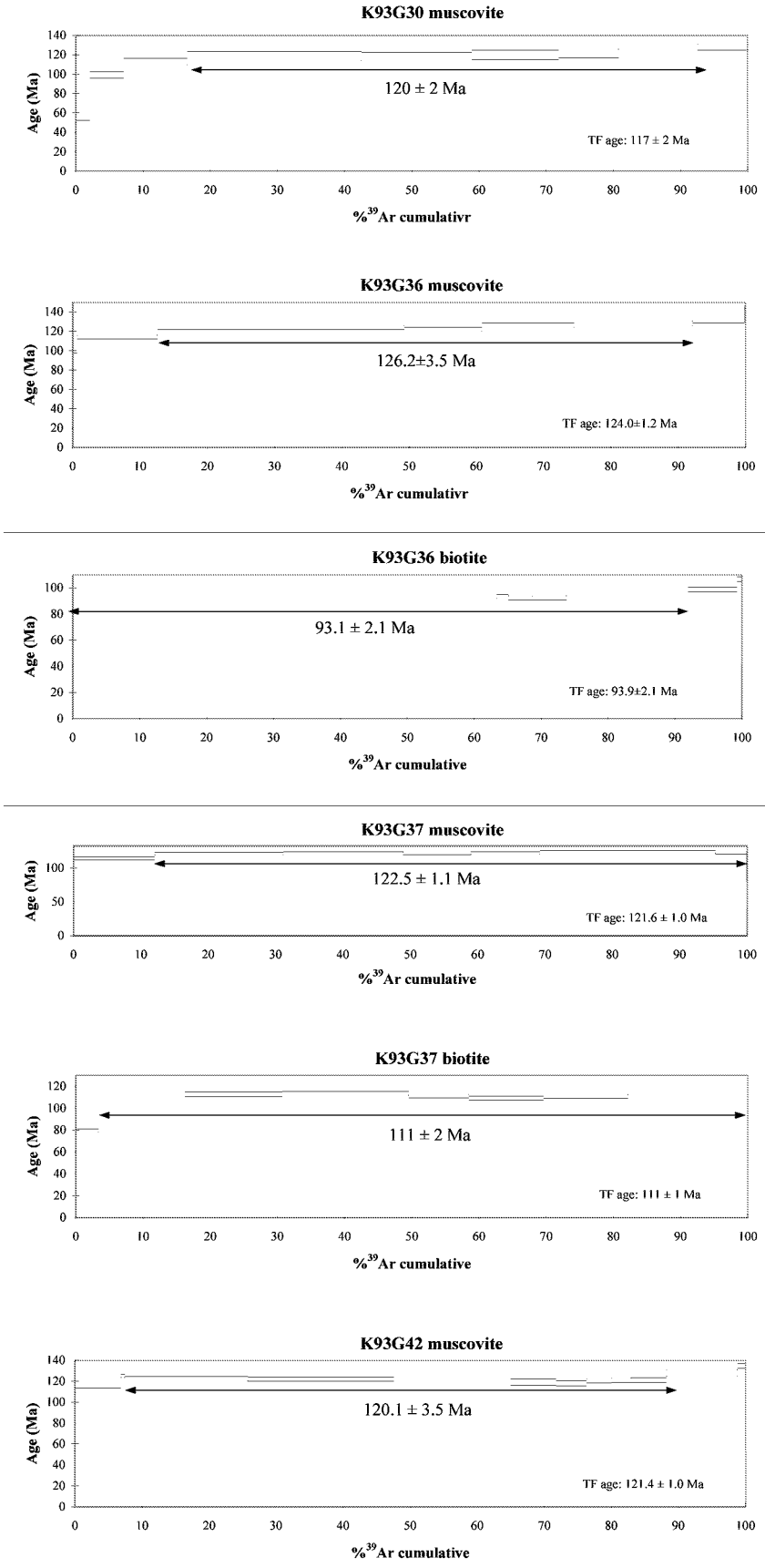

Figure 7
Arnaud et al., 2002

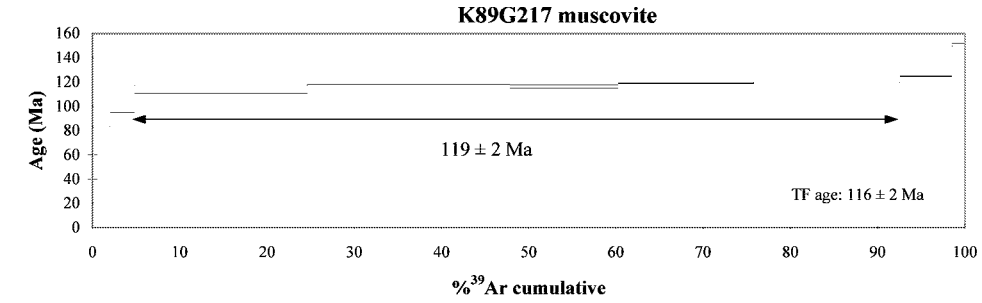

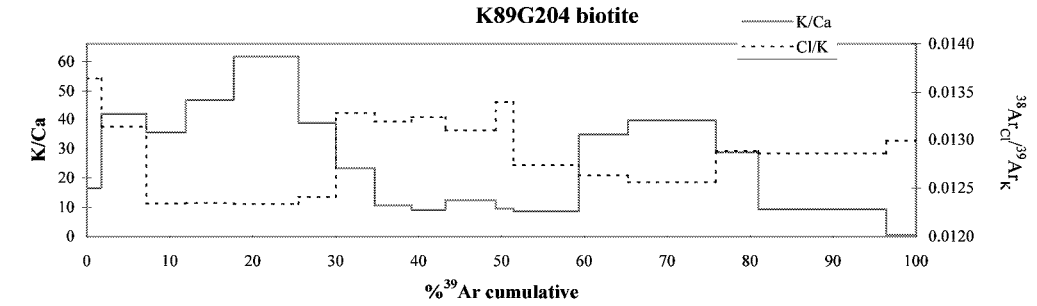

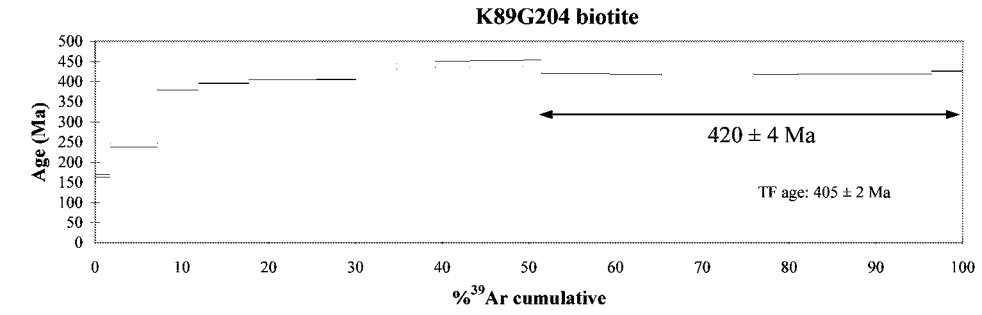

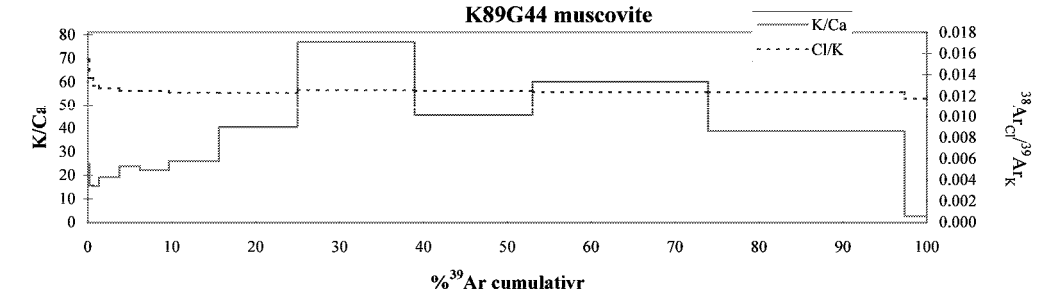

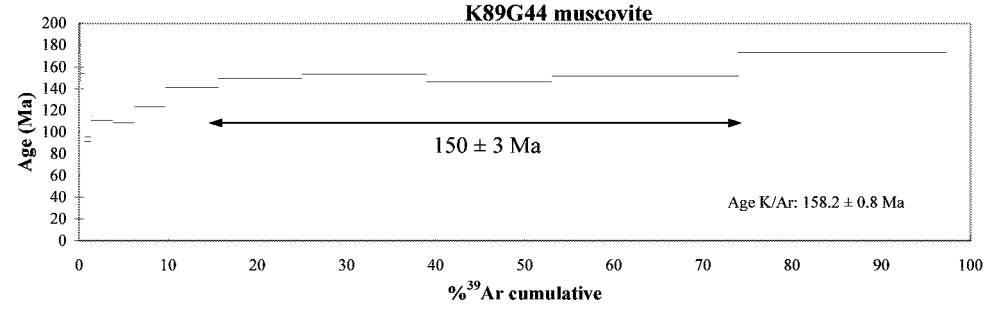

Figure 8a
Arnaud et al., 2002

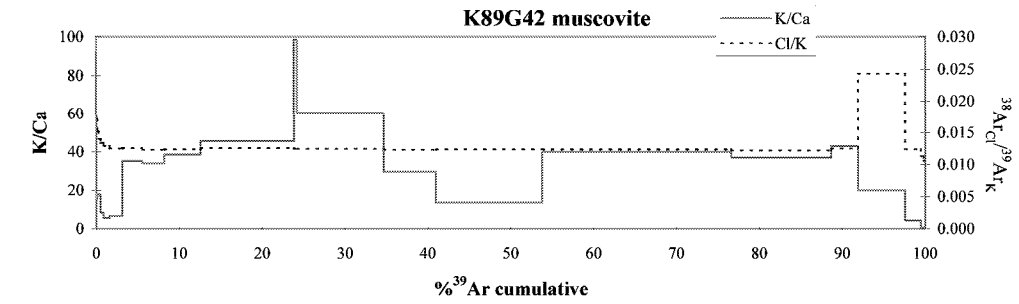

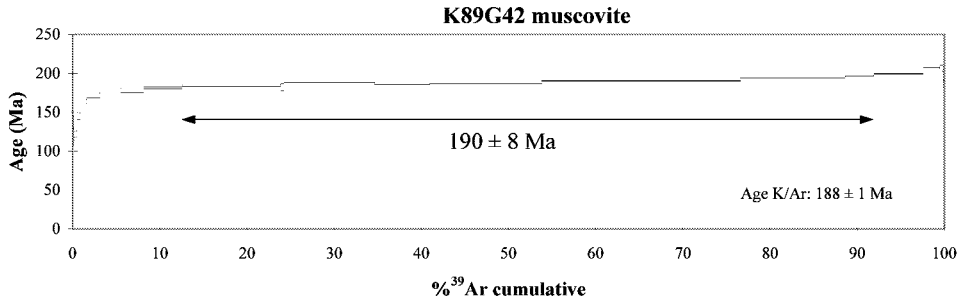

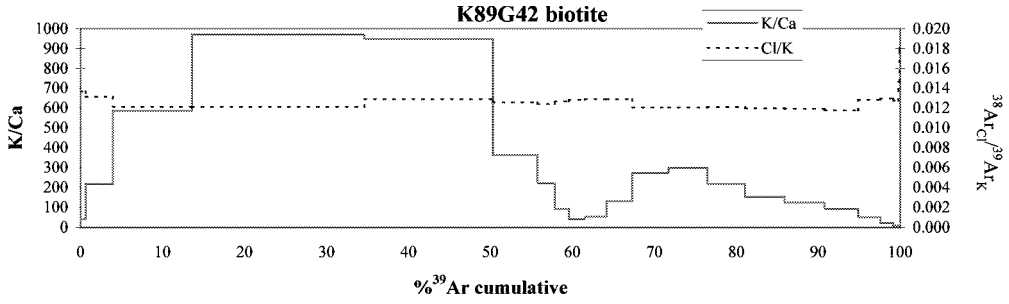

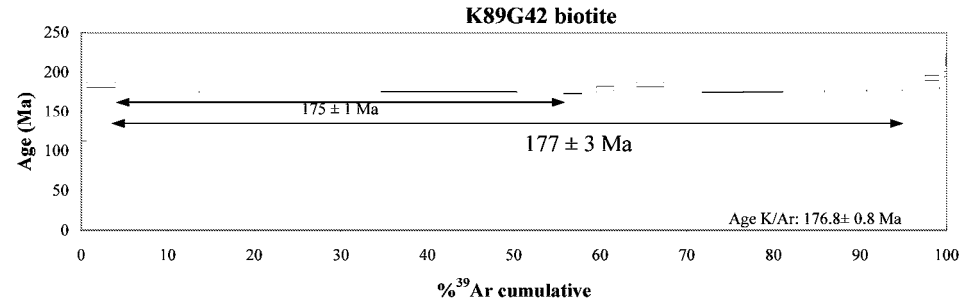

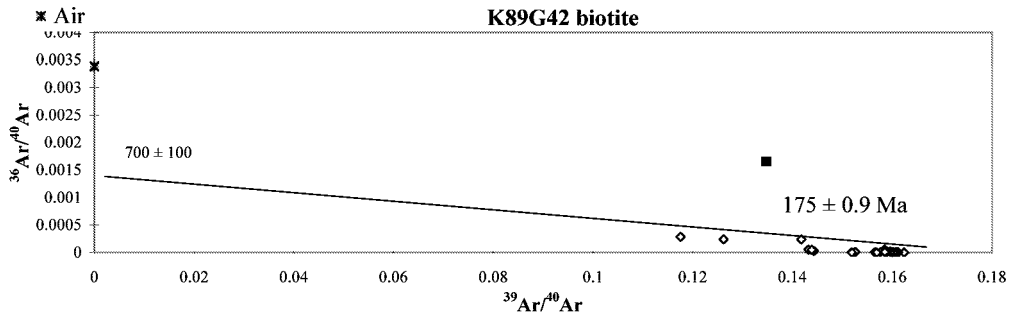

Figure 8b
Arnaud et al., 2002

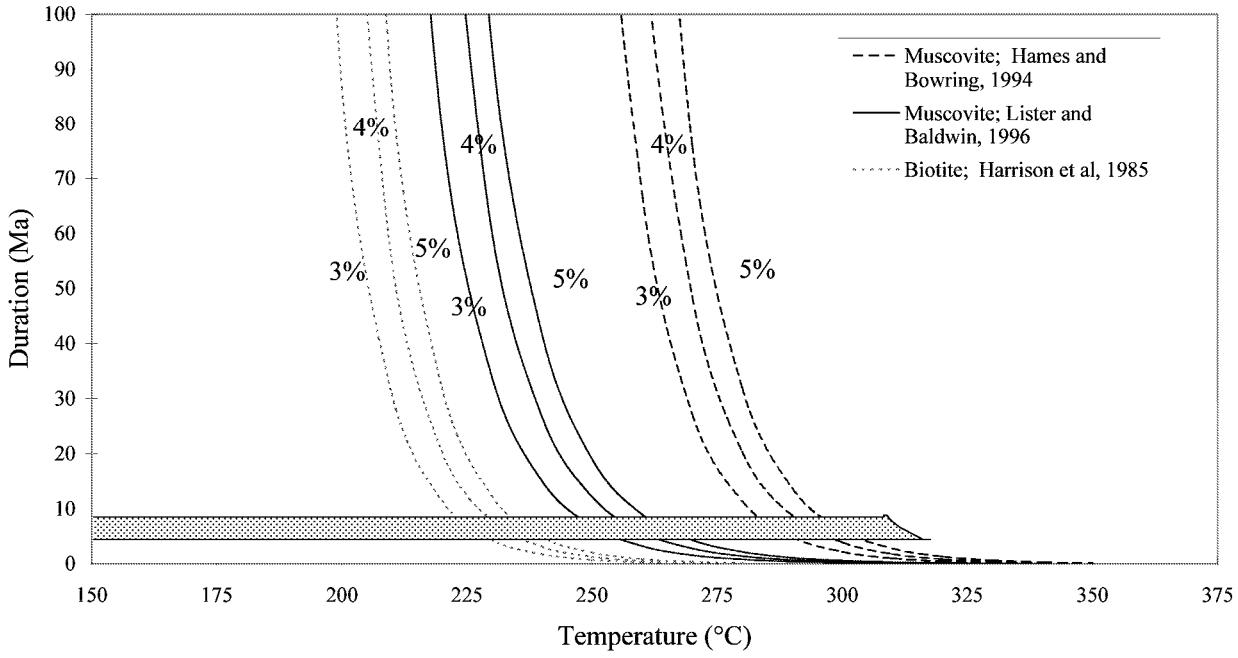

Figure 9
Arnaud et al., 2002

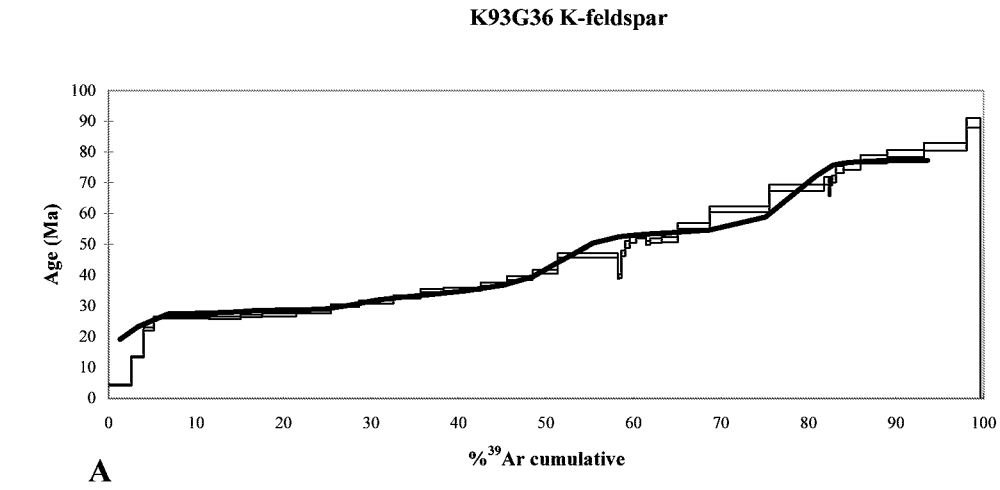

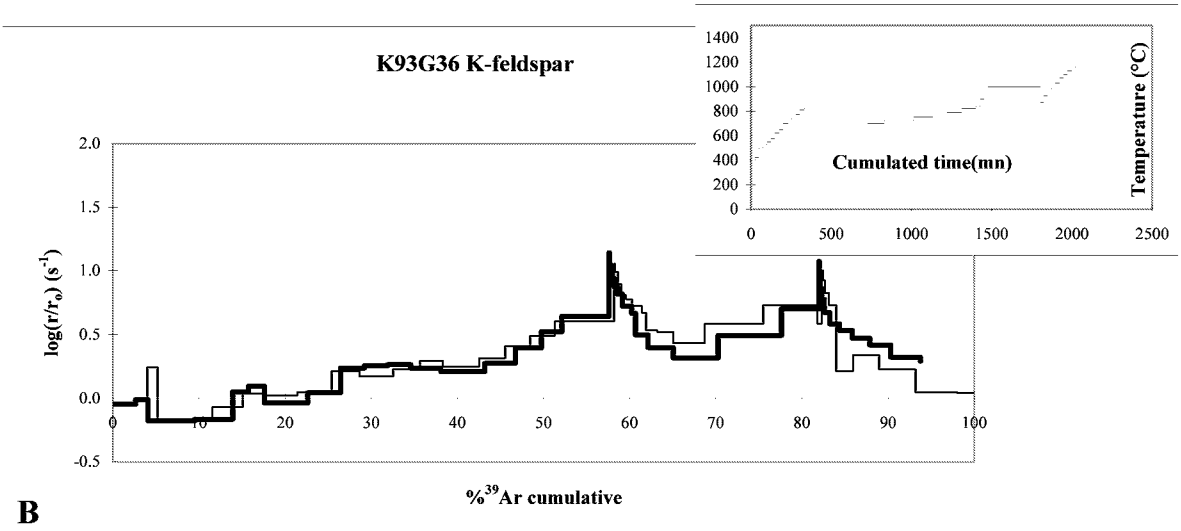

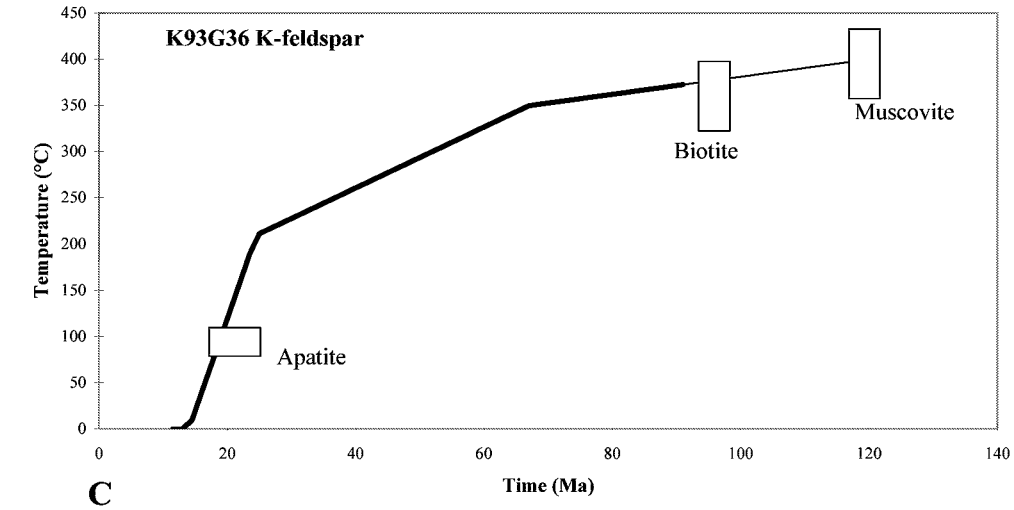

Figure 10a
Arnaud et al., 2002

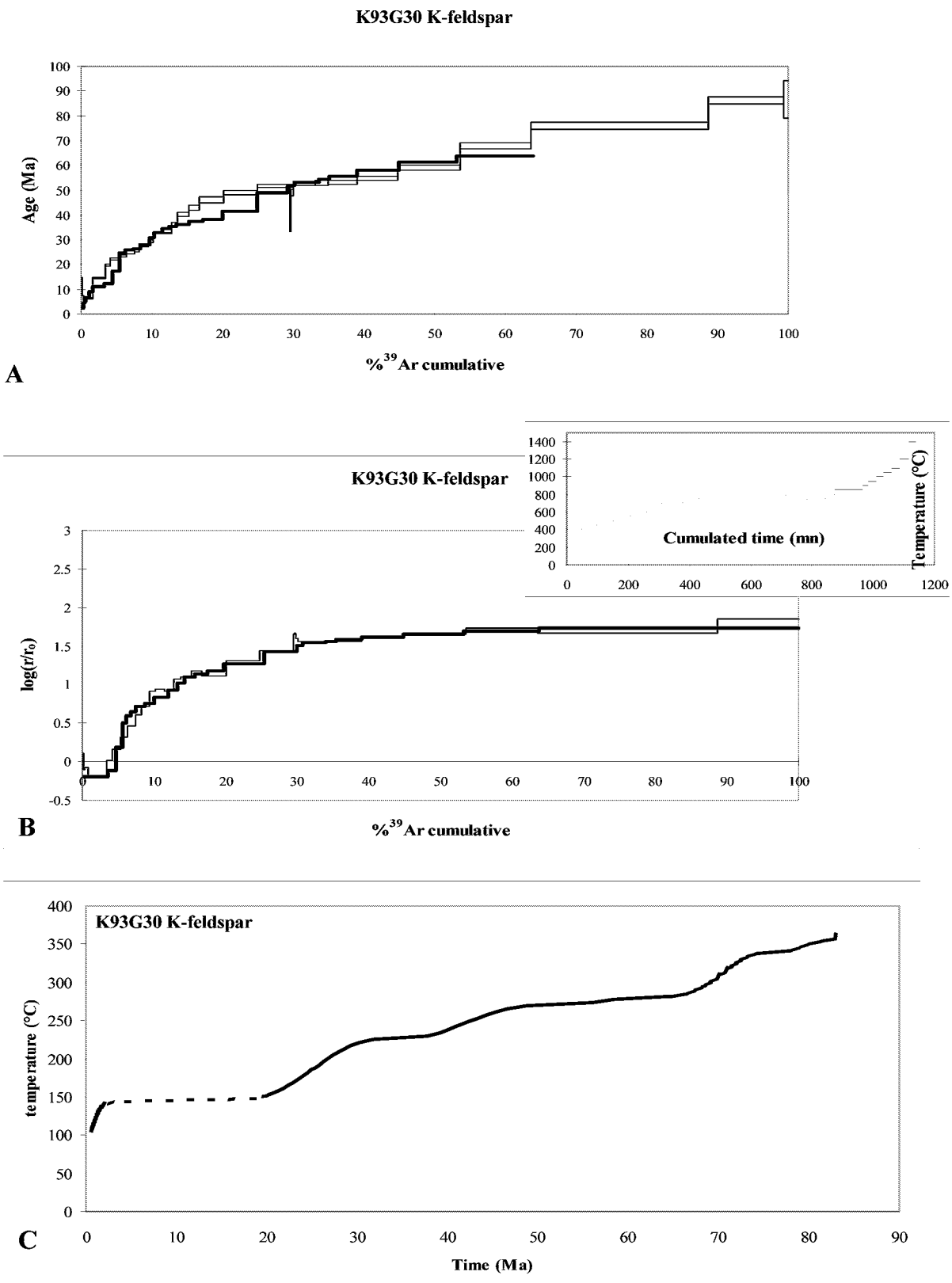

Figure 10b
Arnaud et al., 2002

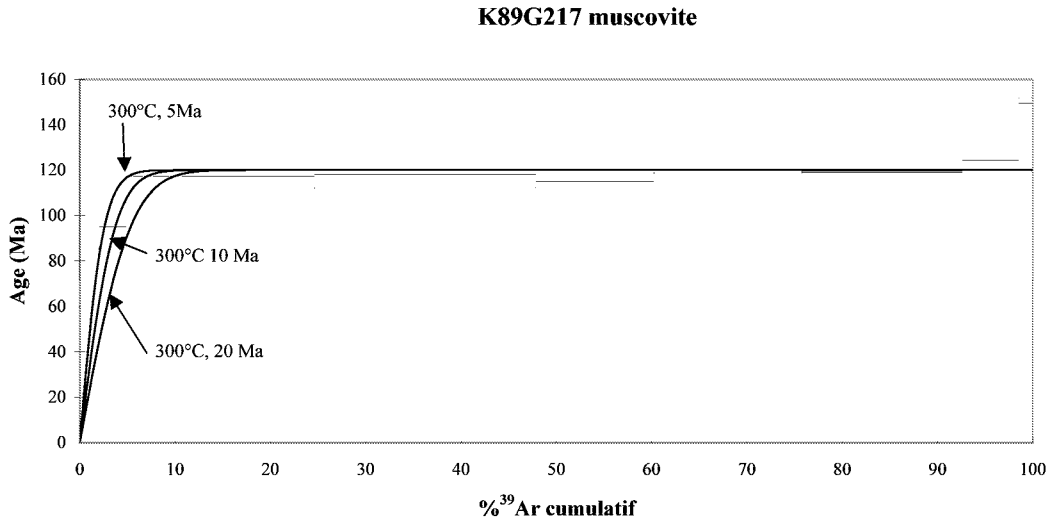

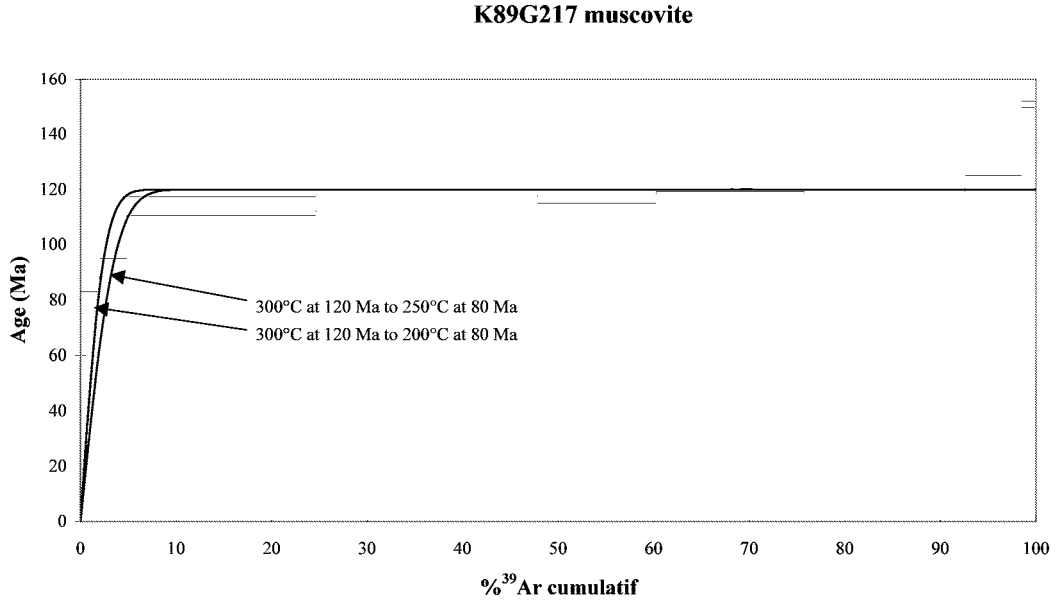

Figure 11
Arnaud et al., 2002

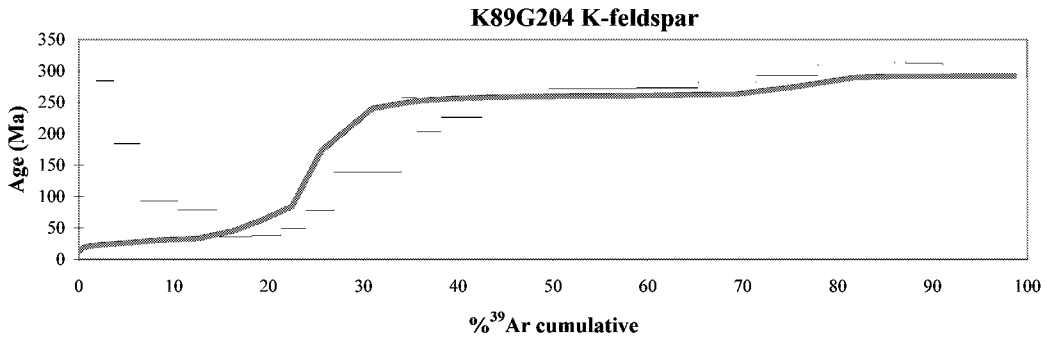

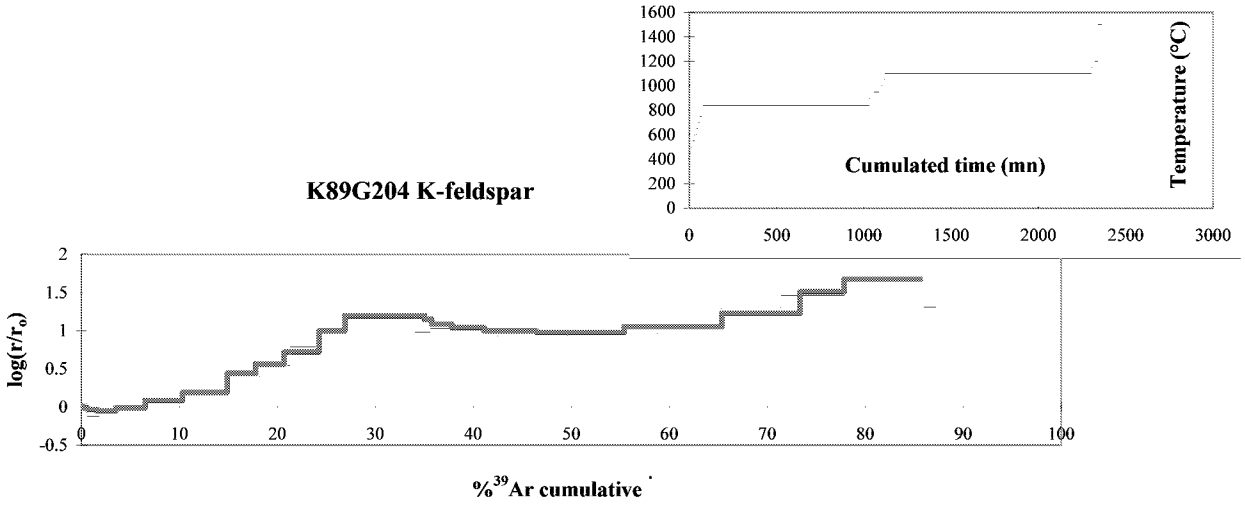

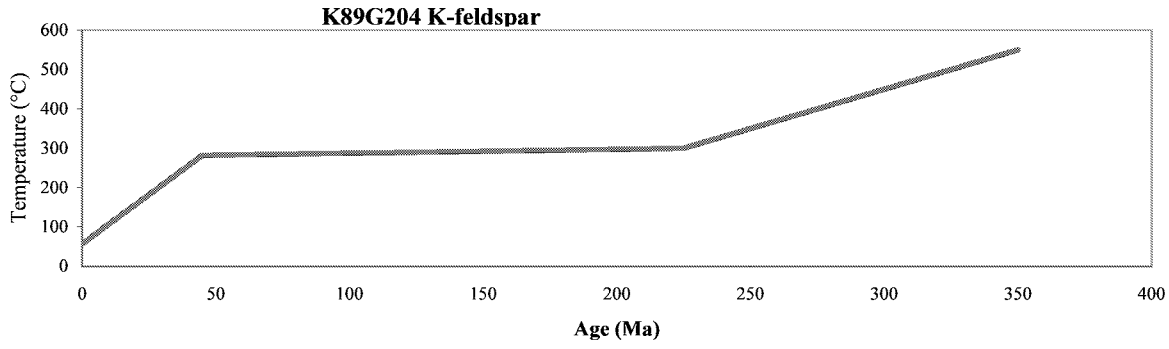

Figure 12 a
Arnaud et al., 2002

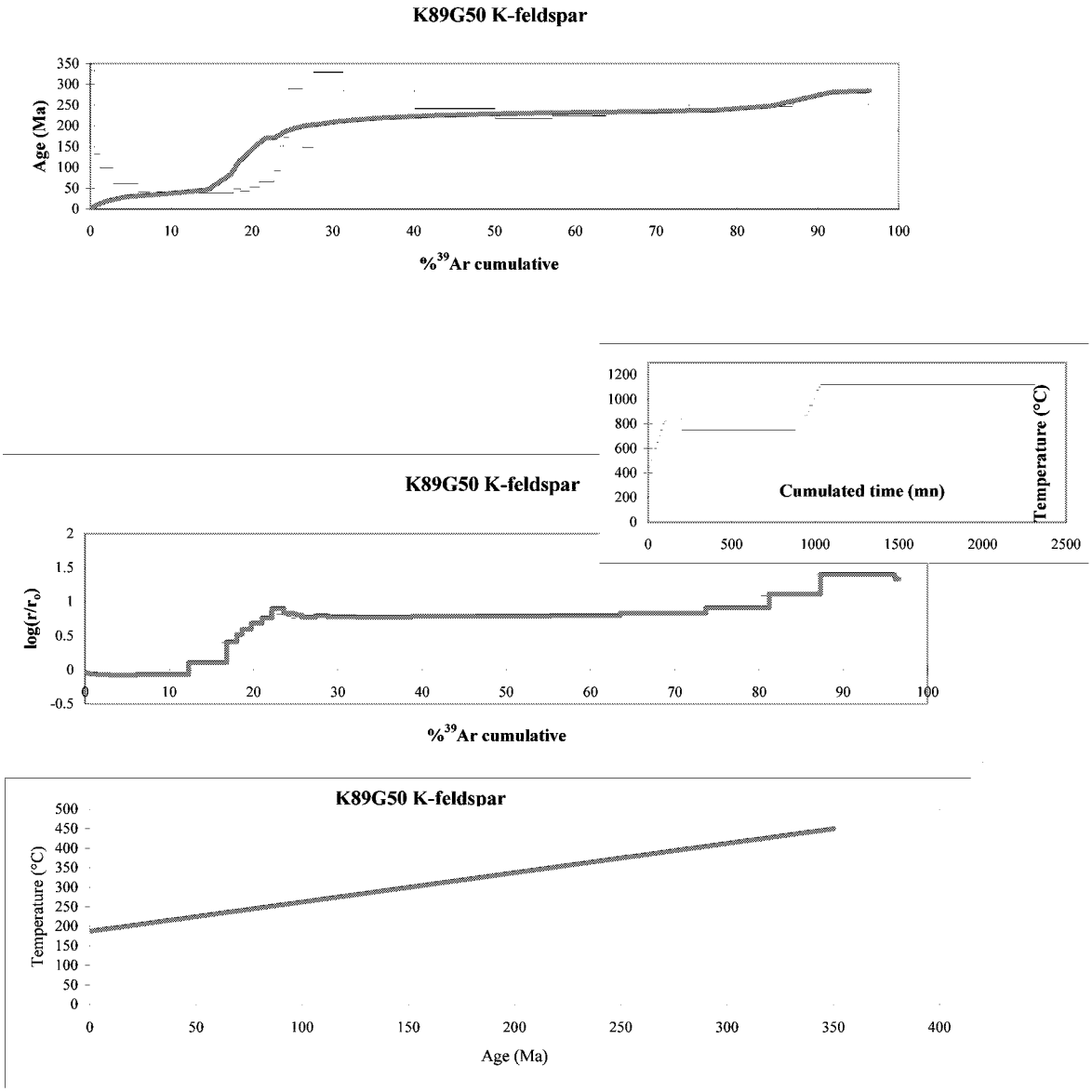

Figure 12 b
Arnaud et al., 2002